

Parametric analysis of ambisonic audio

Contributions to methods, applications and data generation

Author: Andrés Pérez López

TESI DOCTORAL UPF / year 2020

THESIS SUPERVISORS

Dr. Adan Garriga Torres

Dr. Emilia Gómez Gutiérrez

Department of Information and Communication
Technologies



To my cat

Thanks thanks to... **thanks**

Abstract

Due to the recent advances in virtual and augmented reality, ambisonics has emerged as the *de facto* standard for immersive audio. Ambisonic audio can be captured using spherical microphone arrays, which are becoming increasingly popular as well. Yet, many methods for acoustic and microphone array signal processing are not specifically tailored for spherical geometries. Therefore, there is still room for improvements in the field of automatic analysis and description of ambisonic recordings. In the present thesis, we tackle this problem using methods based on the parametric analysis of the sound field. Specifically, we present novel contributions in the scope of blind reverberation time estimation, diffuseness estimation, and sound event localization and detection. Furthermore, several software tools developed for ambisonic dataset generation and management are also presented.

Resum

Ambisonics ha esdevingut l'estàndard d'àudio immersiu als últims anys, afavorit pels avanços en realitat virtual i augmentada. L'àudio ambisonic es pot obtenir mitjançant *arrays* de micròfons esfèrics, que també són cada vegada més populars. Tot i això, la majoria de mètodes acústics i de processament de senyal basats en *arrays* de micròfons no estan adaptats al cas específic de geometries esfèriques. Per tant, encara hi ha moltes possibilitats de millora en l'àmbit d'anàlisi automàtic i descripció de gravacions ambisonic. En la present tesi plantegem aquest problema basant-nos en l'anàlisi paramètric del camp acústic. Més concretament, presentem contribucions originals en les àrees d'estimació de reverberació, estimació de difusió acústica, i detecció i localització d'esdeveniments sonors. Tanmateix, presentem diverses eines de programari desenvolupades per la generació i manteniment de bases de dades d'àudio ambisonic.

Preface is that really needed?

Contents

List of figures	xvii
------------------------	-------------

List of tables	xix
-----------------------	------------

1 Introduction	1
1.1 Motivation	1
1.2 Problem Description	5
1.3 Scientific Objectives	8
1.4 Outline	8
1.5 Contributions	10
2 Scientific Background	13
2.1 Conventions	13
2.1.1 Reference system	13
2.1.2 Nomenclature	15
2.2 Spherical Harmonics	15
2.2.1 Definition	15
2.2.2 Spherical array processing	17
2.3 Ambisonics	19
2.3.1 Ambisonics Theory	19
2.3.2 Practical considerations	24
2.4 Parametric Spatial Audio Analysis	28
2.5 Spatial Coherence Analysis	32
2.6 Reverberation	33

2.7	Signal Models	37
3	Blind reverberation time estimation	39
3.1	Introduction	39
3.2	Signal Model	40
3.3	Baseline method	41
3.4	Proposed method	42
3.4.1	Dereverberation	43
3.4.2	System Identification	45
3.5	Experimental setup	46
3.5.1	Dataset	46
3.5.2	Setup	47
3.5.3	Evaluation metrics	49
3.6	Results	49
3.7	Conclusion	53
4	Coherence Estimation	55
4.1	Introduction	55
4.1.1	Problem definition	56
4.2	Methods	56
4.2.1	Simulation	56
4.2.2	Recording	57
4.2.3	Data processing and metrics	57
4.3	Results and discussion	58
4.3.1	A-Format	58
4.3.2	B-Format	59
4.4	Conclusions	62
5	Sound Event Localization and Detection	63
5.1	Introduction	63
5.2	SYSTEM DESCRIPTION	64
5.2.1	Single-source estimation	65
5.2.2	Particle tracking	66
5.2.3	Signal filter	68
5.2.4	Event classification	68

5.3	EXPERIMENTS	70
5.3.1	Dataset and baseline system	70
5.3.2	Experimental setup	71
5.3.3	Evaluation metrics	73
5.4	RESULTS	73
5.5	Conclusion	77
6	Data generation and storage	79
6.1	Introduction	79
6.2	MASP: a Python library for multichannel acoustic signal processing	81
6.2.1	Description	81
6.2.2	Related software	83
6.3	SOFA	86
6.3.1	Problem statement	86
6.3.2	Ambisonics Directional Room Impulse Re- sponse as a SOFA convention	86
6.3.3	pysofaconventions	88
6.4	Ambiscaper	89
7	Conclusions	91
7.1	Summary of Contributions	91
7.2	Conclusion	92
7.3	Future work	92

List of Figures

1.1	Number of ambisonic microphones released in last years (from [Wikipedia, 2020]). From left to right, the vertical lines correspond to (i) Oculus acquisition, (ii) Time cover page on VR, (iii) M. Zuckerberg’s speech in MWC, and (iv) Jaunt announcement of shift towards AR.	3
1.2	Venture investments in VR in the period 2014-2018. Adapted from [Fortune, 2019].	5
1.3	General scheme of the B-Format audio generation and analysis framework. Solid lines represent audio signals, while outlined arrows refer to non-audio information.	6
1.4	General scheme of the B-Format audio generation and analysis framework, including the thesis contributions in form of Chapter numbers.	9
2.1	Spherical harmonics up to order $N = 3$. The rows correspond to the spherical harmonics of a given order n , and the columns span all possible degree values.	17
2.2	Magnitude of $\Gamma_n(kR)$ for different ambisonic orders, in the case of (a) rigid sphere, and (b) open sphere configurations. Adapted from [Rafaely, 2004]. . . .	19
2.3	Directive patterns of first-order ambisonic decoding.	23

2.4	Maximum value of each ambisonic channel up to order 5, for all different normalization schemes. Image from [Carpentier, 2017].	26
2.5	Parametric time-frequency spatial audio analysis of a first order ambisonic recording. From top to bottom: 1.) Magnitude spectrogram of the omnidirectional channel. 2.) and 3.) Azimuth and elevation of the estimated instantaneous narrowband DOAs $\Omega(k, n)$. 4.) Instantaneous narrowband diffuseness $\Psi(k, n)$	31
2.6	Room impulse response model, from [Murphy et al., 2017].	34
2.7	Room impulse response model, adapted from http://www.bnoack.com/	37
3.1	Experiment results for <i>speech</i> (left column) and <i>drums</i> (right column) datasets. Estimation error computed for each audio clip.	51
3.2	Experiment results for <i>speech</i> (left column) and <i>drums</i> (right column) datasets. Total estimation error across audio clips and acoustic conditions. Top: boxplot. Bottom: histogram and density plot	52
4.1	<i>A-Format</i> coherence between microphone signals. Left: MSC as a function of the frequency of theoretical, simulated and recorded ((BLD, BRU) , $N = 5$, $I = 64$) signals. Right: mean error $\bar{\epsilon}$ of the recorded signals' MSC (BLD, BRU) compared to the simulated values, for all values of N and I . REDO FIGURE WITH N AND I	58
4.2	Estimated <i>B-Format</i> coherence (Δ) of a simulated diffuse sound field, as a function of the temporal averaging vicinity radius r . Left: $\Delta(k)$ for different values of r , with (coarse) and without (fine) application of radial filters. Right: mean and standard deviation of $\Delta(k)$ as a function of r	59

4.3	<i>B-Format coherence</i> between microphone signals. Left: Δ of simulated and recorded ($N = 5, I = 64$) signals. Right: $\bar{\epsilon}$ of the recorded signals coherence across all values of N and I . REDO FIGURE	61
5.1	Architecture of the proposed methodology.	65
5.2	Estimation of localization and temporal activation. Top: azimuth spectrogram after diffuseness mask; color indicates estimated position of a TF bin passing the single-source test. Bottom: input/output of the particle tracking; the crosses represent the measurement space, and the continuous lines are the resulting events.	67
5.3	Gradient boosting machine learning process. Adding weak estimators allows reducing overall error in the predictions.	69
5.4	Number of occurrences of each event class in the training set, for both proposed methods.	72
5.5	Most representative features in event classifier. . . .	76
6.1	2018 projections of future internet traffic for major programming languages. Adapted from [Robinson, 2017].	80
6.2	Frequency response of an arbitrary spherical array. .	83
6.3	Evaluation of radial filters for an arbitrary spherical microphone array.	84

List of Tables

1.1	List of ambisonic microphones released in recent years (from [Wikipedia, 2020]).	4
2.1	Cartesian and spherical representation of characteristic points along the unit sphere.	14
2.2	Ambisonic decoding: standard values of α_n weightings. Adapted from [Daniel, 2000].	22
2.3	Reverberation time computation: usual reference levels	36
3.1	Baseline system: linear regression parameters	48
3.2	Experiment results	49
5.1	Acoustic features used for classification, grouped by type.	70
5.2	(Hyper-)parameter values.	74
5.3	Evaluation results on the development set.	75
6.1	Features of <i>MASP</i> compared to <i>pyroomacoustics</i>	85

Chapter 1

Introduction

1.1 Motivation

Ambisonics is a spatial audio theory based on the directional decomposition of the sound field. Conceived in its primal form during the 70s [Gerzon, 1973], it was not until the 21st century, with a modern mathematical formulation [Daniel, 2000] and much more computational power available, that it definitely drew the attention of the research community.

Nevertheless, the greatest contributor to the current interest in ambisonics has been the rise of Virtual Reality (VR) in recent years. Although VR focuses primarily on visual cues, the immersive experience might be greatly enhanced by spatial audio [Begault and Trejo, 2000]. In this context, Ambisonics has been rapidly adopted as *de facto* standard for spatial audio transmission, supposedly due to a variety of factors:

Layout independence As opposed to other audio spatialization techniques that rely on specific playback layouts, ambisonics makes use of an intermediate sound field representation, known as *B-Format* (or just ambisonic audio). This representation, often referred to as *scene-based*, can be then further processed to match any playback configuration.

Recording device independence Regardless of the specific characteristics of an ambisonic microphone, the recorded signal is usually converted into B-Format, which effectively represents the standard exchange format.

Ease of manipulations Signal-independent transformations of the ambisonic stream, and specifically rotations, are computationally inexpensive.

Binaural transformation Spatial audio in VR is mostly consumed as binaural; methods for ambisonic to binaural conversion have been known for a long time [Noisternig et al., 2003]. Furthermore, VR headsets can easily provide head rotation information, which can be used in combination with scene rotations to provide head-locked audio, which greatly improves localization accuracy and immersiveness [Begault and Trejo, 2000]. This is a key feature of ambisonics when compared to static binaural recordings.

Coming back to the Virtual Reality popularity, the following three events might be representative of the growth that it experienced in the second half of the 2010s: (i) the billionaire acquisition by Facebook of the VR headset manufacturer Oculus, in March 2014 [Facebook, 2014]; (ii) the Time cover page devoted to VR: “*The surprising joy of Virtual Reality. And why it’s about to change the world*” (August 2015) [Time, 2015]; and (iii) M. Zuckerberg’s invited talk at the *Samsung Unpacked* event within the World Mobile Congress 2016 in Barcelona: “*VR is the next platform where anyone can experience anything they want*” [BBCNews, 2016].

Given this context, many microphone manufacturers and audio-related companies have followed the industry trend in the search for new markets. Only in the interval 2016-2019, 12 different ambisonic microphones have reached the market (Figure 1.1) — a greater amount than all previous existing ambisonic microphones together. A comprehensive list of recent ambisonic microphone releases is shown in 1.1.

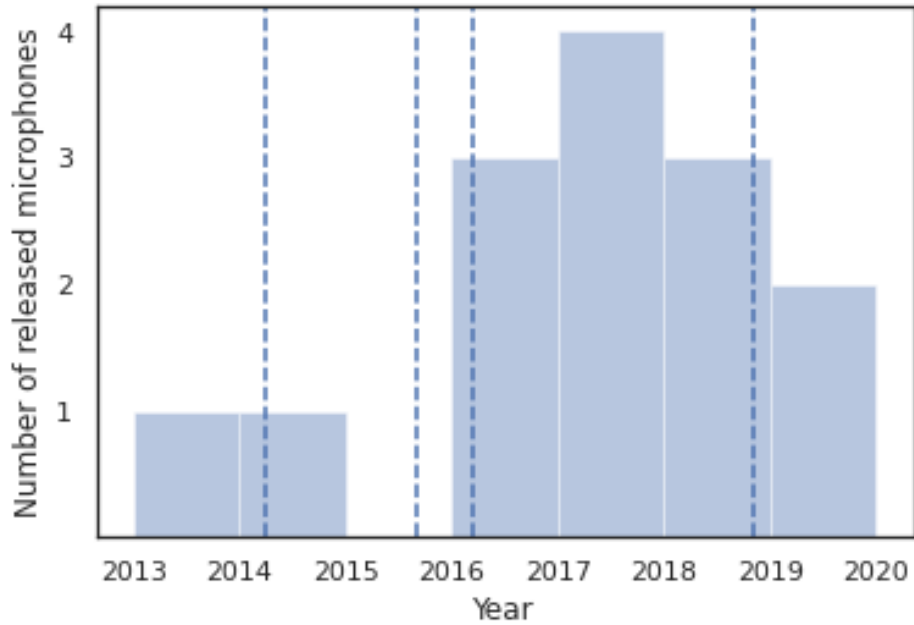


Figure 1.1: Number of ambisonic microphones released in last years (from [Wikipedia, 2020]). From left to right, the vertical lines correspond to (i) Oculus acquisition, (ii) Time cover page on VR, (iii) M. Zuckerberg’s speech in MWC, and (iv) Jaunt announcement of shift towards AR.

At the present time, however, the high expectations in VR have significantly lowered, as shown in Figure 1.2. This is due to a variety of reasons, including lack of interesting content and the high production cost of the headsets [Fortune, 2019]. The change of focus of Jaunt (formerly one of the biggest VR film production companies) towards Augmented Reality (AR), as of October 2018, might be a paradigmatic example of this tendency [TheVerge, 2018].

In any case, the current high availability and affordability of ambisonic microphones brings new challenges from the signal processing perspective. More specifically, ambisonic microphones

Table 1.1: List of ambisonic microphones released in recent years (from [[Wikipedia, 2020](#)]).

Manufacturer	Model	Year	Order
MH Acoustics	EigenMike	2013	4
Brahma	(Brahma)	2014	1
Sennheiser	Ambeo	2016	1
Twirling	720 VR	2016	1
Zoom	H2n	2016	1
Zylia	ZM-1	2017	3
Twirling	720 Lite	2017	1
Ricoh	TA-1	2017	1
Nevaton	Nevaton VR	2017	1
Rode	Rode NT-SF1	2018	1
CoreSound	OctoMic	2018	2
Zoom	H3-VR	2018	1
Brahma	Brahma 8	2019	2
Voyage Audio	Spatial Mic	2019	2

conform a subset of near-coincident spherical microphone arrays, a category which possesses some specific characteristics.

Although the VR momentum has also reached spherical microphone array processing, many challenges remain still open, and the number of research works specifically focusing on such geometry are low yet. Besides that, the growing interest in AR poses new problems related to acoustical signal processing. But since ambisonics is still the standard choice for immersive audio, existing solutions might be successfully adapted.

Lastly, the advance in signal processing methods for ambisonics can give rise to applications that enhance the work of immersive audio producers, providing meaningful information about the recorded scenes and automating some of the repetitive tasks, thus allowing a more flexible and creative workflow.

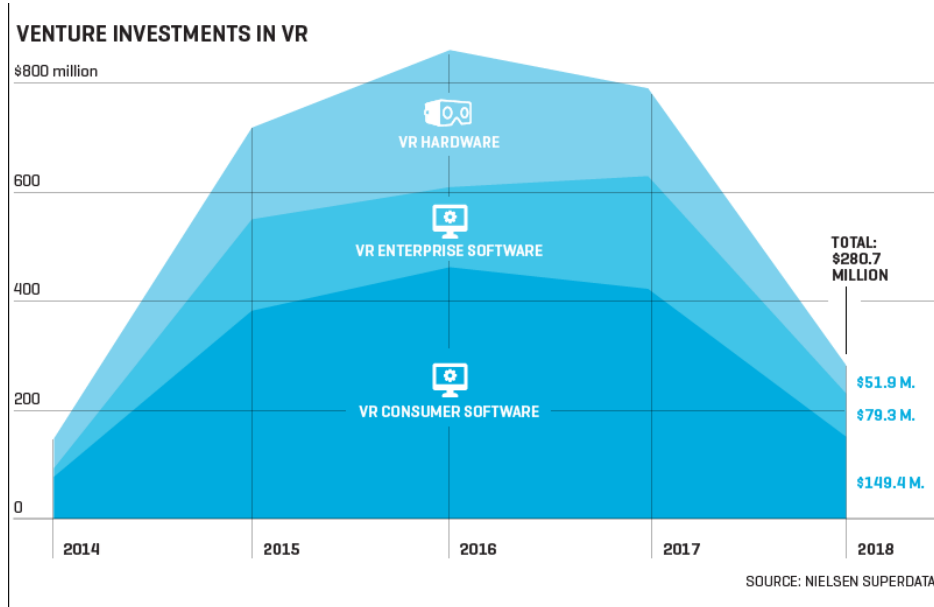


Figure 1.2: Venture investments in VR in the period 2014-2018. Adapted from [Fortune, 2019].

1.2 Problem Description

The scientific context of the work developed in the present dissertation is depicted in Figure 1.3, which has been inspired by [Jarrett et al., 2017]. As we can observe, there are two main topics related with B-Format audio: *generation* and *analysis*, with the signal flow going from the former to the latter. Although the conceptual approach of the scheme might be very similar for any type of audio, the specific spatial information conveyed by the ambisonic signal places an emphasis on the informed analysis and description of the sound scene.

The problem of B-Format generation is mostly related with dataset generation, which is a common issue for many audio sig-

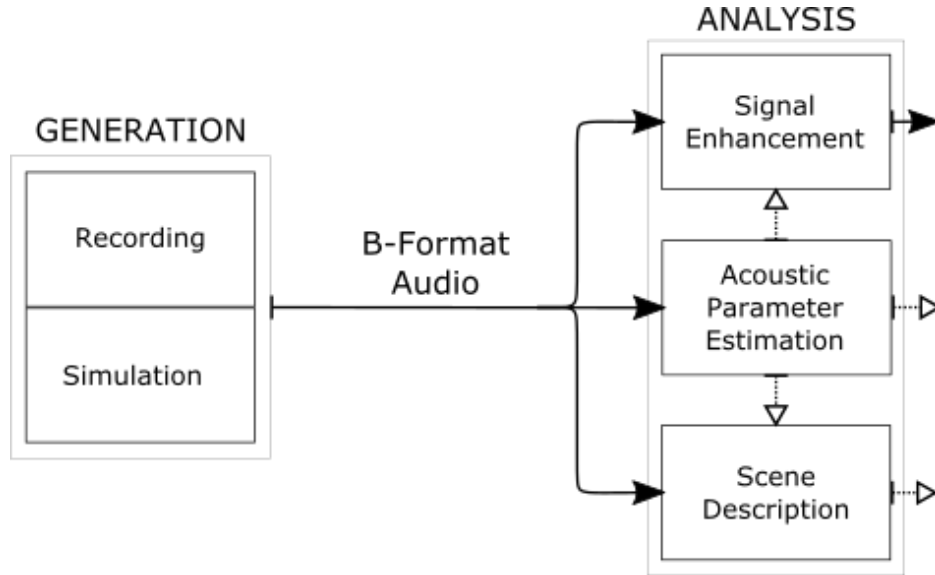


Figure 1.3: General scheme of the B-Format audio generation and analysis framework. Solid lines represent audio signals, while outlined arrows refer to non-audio information.

nal processing problems. In our case, we consider two different approaches to the data generation problem:

Recording Using spherical microphone arrays for the recording of ambisonic material.

Simulation Using numerical methods for the simulation of acoustic scenes.

While recordings are by definition more similar to real scenarios, they are expensive to perform, and can only provide a limited set of parameter possibilities. Simulations, on the other hand, have the potential to cover any desired condition. Therefore, it is of our interest to consider the strengths of both signal generation paths.

B-Format analysis has been divided into three different categories:

Acoustic Parameter Estimation Low-level analysis of the sound field, which yields quantitative information about different acoustic parameters used to model the acoustic scene.

Signal Enhancement Modification of the sound field in order to obtain a set of output signals with desired attributes.

Scene Description Textual representation of different high-level characteristics of the sound field.

The knowledge about the acoustic parameters of a sound field can be considered either as a goal by itself, or alternatively as a pre-processing step which complements the other analysis categories. Examples of typical estimated acoustic parameters are the *Direction-of-Arrival* (DOA), the sound field diffuseness, or the reverberation time of the enclosure [Jarrett et al., 2017].

There are a variety of well known signal enhancement problems, including dereverberation [Braun, 2018], source separation [Gannot et al., 2017], or foreground-background segmentation [Stefanakis and Mouchtaris, 2015]. As it has been shown, many of them benefit (or even depend) from the knowledge derived by the acoustic parameter estimation step.

Finally, under the scene description typology we can find a set of applications that provide abstract representations of the sound scene under analysis. Most of the recent research performed in this scope is grouped around the Detection and Classification of Acoustic Scenes and Events (DCASE) community¹. Examples of the problems under consideration are acoustic scene classification [Mesaros et al., 2018], sound event localization and detection [Adavanne et al., 2018] or audio captioning [Drossos et al., 2017].

¹http://dcase.community/community_info

1.3 Scientific Objectives

The list that follows concentrates the main scientific objectives to be developed on this thesis:

- To develop methods for the characterisation of acoustic parameters from recordings originated from ambisonic microphones.
- To propose methodologies for sound event localization and detection in ambisonic domain which are grounded on spatial parametric analysis.
- To contribute in the generation and storage of ambisonic sound scenes, for their usage in controlled experimental environments.

1.4 Outline

The present dissertation is organised as follows.

Chapter 2 introduces the basic concepts that will be developed throughout this thesis, including spherical harmonics and ambisonics, coherence estimation, parametric analysis or room acoustics. The Chapter also defines the signal models and the mathematical terminology.

Chapters 3, 4 and 5 develop the most significant academic contributions of this thesis. **Chapter 3** presents a novel method for blind reverberation time in ambisonic recordings. To the best of our knowledge, this is the first method proposal specifically focusing on that problem. The method is based on a Multichannel Auto-Regressive model of the late reverberation, which allows for an effective dereverberation of the ambisonic sound scene, and enables computation of the reverberation time from an estimation of the room impulse response. The evaluation metrics show a method performance similar to other state-of-the-art methods. **Chapter 4**

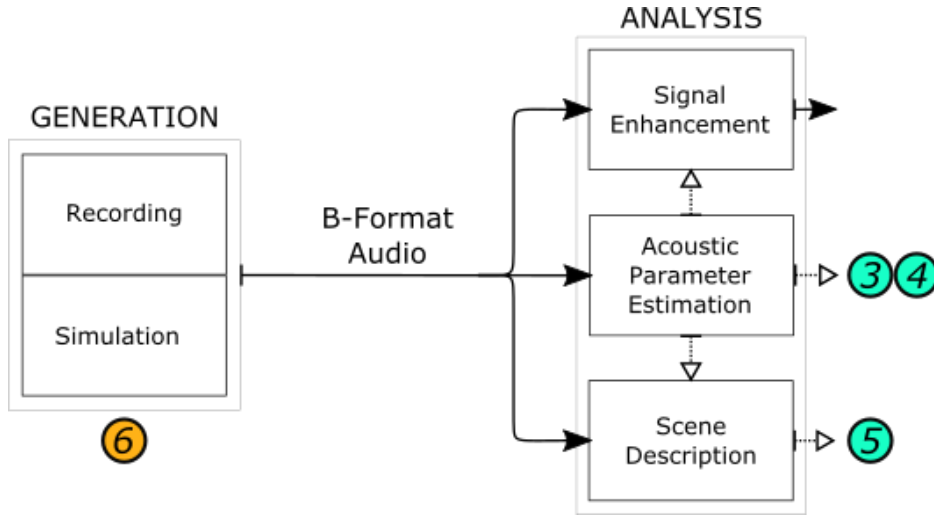


Figure 1.4: General scheme of the B-Format audio generation and analysis framework, including the thesis contributions in form of Chapter numbers.

analyses the response of tetrahedral microphone arrays, which are the simplest and most common form of ambisonic microphones, under spherically isotropic sound field. The analysis is performed using both simulated and recorded diffuse field, and the results quantify the differences between ideal and real values under a variety of conditions and estimators. In **Chapter 5**, a complete system for Sound Event Localization and Detection of ambisonic sound scenes is described. The algorithm comprises two different parts. First, a parametric analysis is performed on the ambisonic signal. The analysis yields spatial localization and temporal activities of the sound events present in the scene. Then, each of those events is assigned to a class label by means of a deep-learning classifier. The method is able to perform in a similar way to the baseline system, while greatly improving its localization capabilities.

Finally, **Chapter 6** presents some libraries and software utilities developed throughout this thesis. All the code has been publicly

released under open source licenses. The libraries include utilities for the creation of datasets, the storage and exchange of impulse response files in a standard way, and the implementation of convenience tools for acoustic and microphone array signal processing analysis. Although the libraries do not directly involve any scientific contribution, they can be a great help for scientific and innovative purposes; given the industrial nature of this thesis, we have considered relevant to include them in the present dissertation.

In order to provide a schematic representation of the thesis structure and scope, Figure 1.4 features the problem structure stated in Figure 1.3, with the addition of the Chapter numbers with the contributions of this thesis.

1.5 Contributions

In the following list we show the main scientific contributions of this dissertation, organised by Chapters:

- Chapter 3:
"Blind reverberation time estimation from ambisonic recordings". A. Pérez-López, A. Politis and E. Gómez. Submitted to *IEEE 22nd International Workshop on Multimedia Signal Processing*, 2020.
- Chapter 4:
"Analysis of spherical isotropic noise fields with an A-Format tetrahedral microphone". A. Pérez-López and N. Stefanakis. *The Journal of the Acoustical Society of America* 146.4 (2019): EL329-EL334.
- Chapter 5:

"PAPAFIL: a low complexity sound event localization and detection method with parametric particle filtering and gradient boosting". A. Pérez-López and R. Ibañez-Usach. Submitted to *Detection and Classification of Acoustic Scenes and Events 2020 Workshop (DCASE2020)*.

"A hybrid parametric-deep learning approach for sound event localization and detection". A. Pérez-López, E. Fonseca and X. Serra. In *Proceedings of the Detection and Classification of Acoustic Scenes and Events 2019 Workshop (DCASE2019)*.

- Chapter 6:

"Ambiscaper: A Tool for Automatic Generation and Annotation of Reverberant Ambisonics Sound Scenes".

A. Pérez-López. In *16th International Workshop on Acoustic Signal Enhancement (IWAENC)*. IEEE, 2018.

"Ambisonics directional room impulse response as a new convention of the spatially oriented format for acoustics".

A. Pérez-López and J. De Muynke. In *Audio Engineering Society Convention 144*. Audio Engineering Society, 2018.

"pysofaconventions, a Python API for SOFA". A. Pérez-López. In *Audio Engineering Society Convention 148*. Audio Engineering Society, 2020.

"A Python library for Multichannel Acoustic Signal Processing". A. Pérez-López and A. Politis. In *Audio Engineering Society Convention 148*. Audio Engineering Society, 2020.

Moreover, although not strictly aligned with the research direction of this thesis, the author has collaborated in the following publications:

- **"Sound event localization and detection based on CRNN using dense rectangular filters and channel rotation data augmentation".** F. Ronchini, D. Arteaga and A. Pérez-López.

Submitted to *Detection and Classification of Acoustic Scenes and Events 2020 Workshop (DCASE2020)*.

Finally, as a result of the development of this thesis, the following open-source libraries have been implemented and released. All of them are available through the author’s GitHub page²:

- [ambisonic_rt_estimation](#)
- [DCASE2020](#)
- [DCASE2019_task3](#)
- [ambiscaper](#)
- [pysofaconventions](#)
- [masp: Multichannel Acoustic Signal Processing library](#)

²<https://github.com/andresperezlopez>

Chapter 2

Scientific Background

2.1 Conventions

2.1.1 Reference system

In what follows, we will make use of a right-handed coordinate system, where the positive x -axis points towards the *front*, the positive y -axis points towards the *left*, and the positive z -axis points towards the *zenith* (North Pole).

Any position in the unit sphere may be described in spherical coordinates by two angles: the *inclination* angle ϑ , which accounts for the aperture with respect to the z -axis, and the *azimuth* angle φ , which represents the counter-clockwise angle with respect to the x -axis from the top-view. The value ranges are $0 \leq \vartheta \leq \pi$ for the inclination, and $0 \leq \varphi \leq 2\pi$ for the azimuth.

Table 2.1 shows the spherical coordinate values for some reference points on the unit sphere. Notice that the poles ($\vartheta = \pm\pi$) are a special case for the spherical coordinate system – in that case, the azimuth angle is not defined.

The transformation between spherical and cartesian coordinate

Table 2.1: Cartesian and spherical representation of characteristic points along the unit sphere.

Position	Cartesian	ϑ	φ
front	$[1, 0, 0]$	$\pi/2$	0
back	$[-1, 0, 0]$	$\pi/2$	π
left	$[0, 1, 0]$	$\pi/2$	$\pi/2$
right	$[0, -1, 0]$	$\pi/2$	$-\pi/2$
zenith	$[0, 0, 1]$	0	*
nadir	$[0, 0, -1]$	π	*

systems is given by the following relationship:

$$\begin{aligned}
 x &= \cos \varphi \sin \vartheta \\
 y &= \sin \varphi \sin \vartheta \\
 z &= \cos \vartheta
 \end{aligned}
 \tag{2.1}$$

The *elevation* angle θ provides an alternative way of describing the relationship with respect to the z -axis. θ is defined as the aperture with respect to the xy -plane, with positive values towards the positive z -axis. The relationship between elevation and inclination angles is:

$$\theta = \pi/2 - \vartheta
 \tag{2.2}$$

For the sake of compactness, a point in the unit sphere will be often represented by $\Omega = (\vartheta, \varphi)$.

Given the periodic nature of the azimuth angle, the descriptive statistic operations applied to ϑ will refer to the 2π -periodic version or the operator; this situation does not affect the inclination/elevation coordinate.

2.1.2 Nomenclature

is this name correct? Throughout the Thesis, we refer to time-domain signals with lowercase, e.g. $x(t)$, with t as the time index.

Time-domain signals transformed by the Short-Time Fourier Transform (STFT) are represented with uppercase, e.g. $X(k, n)$, where k is the frequency bin index, and n the time frame index.

Multichannel signals are in general denoted by a subscript variable index, usually with the letter m ; for example, $x_m(t)$ or $X_m(k, n)$. Signals with an integer subscript index, such as $x_0(t)$, represent a specific channel of the corresponding multichannel signal.

In the context of ambisonic, subscripts and superscripts are used in signal names with a specific meaning; check Section 2.3 for a detailed explanation.

Vector notation is represented with boldface characters, e.g. $\mathbf{X}(k, n)$. When used, the way to construct the vectors will be specified.

2.2 Spherical Harmonics

2.2.1 Definition

Spherical harmonics are continuous functions defined on the sphere surface. Due to their mathematical properties, any spherical function can be decomposed as a combination of spherical harmonics, in what is known as the *Spherical Harmonics Expansion* [Jarrett et al., 2017].

Many different spherical harmonic definitions exist in the literature, with minor variations among them. In the following, we will use the real-valued, fully normalized spherical harmonics as defined by [Zotter and Frank, 2019]:

$$Y_n^m(\varphi, \vartheta) = N_n^{|m|} P_n^{|m|}(\cos(\vartheta)) \Phi_m(\varphi), \quad (2.3)$$

where the *normalization factor* N_n^m is:

$$N_n^m = (-1)^m \sqrt{\frac{2n+1}{2} \frac{(n-m)!}{(n+m)!}} \quad (2.4)$$

the *Legendre polynomials* P_n^m are defined as:

$$P_{n+1}^m = \begin{cases} \frac{2n+1}{n-m+1} x P_n^m, & \text{for } n = m, \\ \frac{2n+1}{n-m+1} x P_n^m - \frac{n+m}{n-m+1} P_{n-1}^m & \text{else,} \end{cases} \quad (2.5)$$

with $P_n^n = \frac{(-1)^n (2n)!}{2^n n!} \sqrt{1-x^2}$ and the initial term $P_0^0 = 1$, and Φ_m is the azimuthal part of the spherical harmonics:

$$\Phi_m(\varphi) = \frac{1}{\sqrt{2\pi}} \begin{cases} \sqrt{2} \sin(|m|\varphi), & \text{for } m < 0, \\ 1, & \text{for } m = 0, \\ \sqrt{2} \cos(m\varphi), & \text{for } m > 0. \end{cases} \quad (2.6)$$

One of the properties of the spherical harmonics is orthonormality on the sphere surface:

$$\int_{\mathbb{S}^2} Y_n^m(\varphi, \vartheta) Y_{n'}^{m'}(\varphi, \vartheta) d\cos\vartheta d\varphi = \delta_{nn'} \delta_{mm'}, \quad (2.7)$$

where δ_{xy} represents the Kronecker delta operator:

$$\delta_{xy} = \begin{cases} 1, & \text{if } x = y, \\ 0, & \text{else.} \end{cases} \quad (2.8)$$

The spherical harmonics depend on the *order* $n \geq 0$ and the *degree* m , $|m| \leq n$ for each value of n . In practice, the maximum order N , $n \leq N$ determines the spatial resolution of the sound field expansion.

Through the spherical harmonic expansion, any sound field may be represented with a limited spatial resolution by the finite combination of all spherical harmonics up to order N . For a given order n , the number of spherical harmonic functions is $2n+1$. With

the accumulation of all orders up to N , the total number of spherical harmonics is given by $M = (N+1)^2$. Figure 2.1 depicts all spherical harmonics from orders 0 to 3.

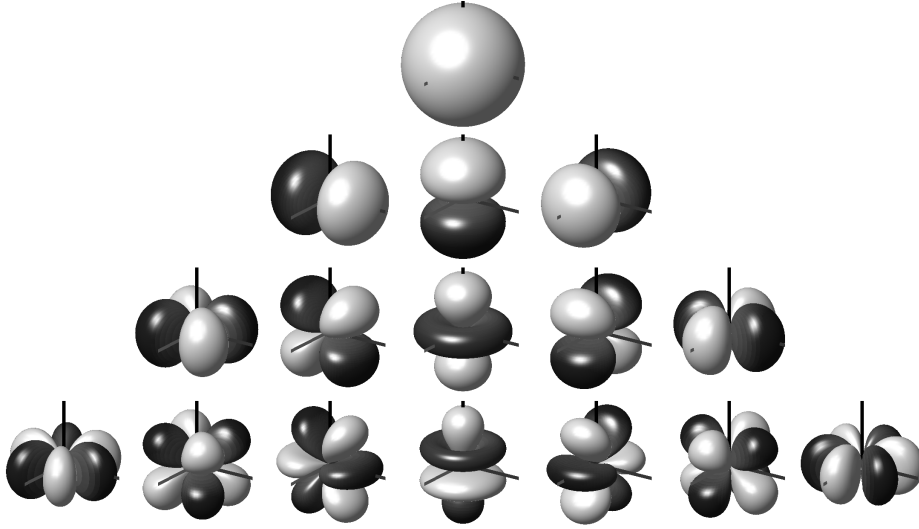


Figure 2.1: Spherical harmonics up to order $N = 3$. The rows correspond to the spherical harmonics of a given order n , and the columns span all possible degree values.

2.2.2 Spherical array processing

Let us consider a sound field captured with a spherical microphone array, which contains Q capsules distributed around a spherical surface of radius R at the positions $\Omega_q, 1 \leq q \leq Q$. The captured frequency-domain signals $X_q(k)$ can be represented as the spherical harmonic domain signals $X_n^m(k)$ through the spherical harmonic transform of order n and degree m [Moreau et al., 2006]:

$$X_n^m(k) = \sum_{q=1}^Q X_q(k) Y_n^m(\Omega_q) \Gamma_n(kR), \quad (2.9)$$

is that actually valid? or Y should be the complex-valued spherical harmonics?

where the term $\Gamma_n(kR)$ models the radial transfer function, and depends on a number of factors, being the *sphere configuration* one of the most prominent considerations. Sphere configuration, in its basic form, refers to the physical properties of the baffle where the capsules are mounted, and it can be either *open* or *rigid*. While open configuration is the simplest solution, it might present numerical problems in the form of zeros in its frequency response. Conversely, a rigid baffle interferes with the sound field and might create undesired interferences, but it improves the numerical condition from the open case. Fig. 2.2 shows the simulated magnitude response of $\Gamma_n(kR)$ for a spherical array considering both configurations. The reader is referred to [Moreau et al., 2006] and [Rafaely, 2004] for a deeper insight into the topic of spherical microphone array design.

By using the model from Eq. 2.9, the maximum spherical harmonic order N that can be retrieved with negligible spatial aliasing depends on the number of microphone capsules [Moreau et al., 2006]:

$$N \geq (Q + 1)^2. \quad (2.10)$$

Furthermore, the sphere radius R has also an effect on the operational bandwidth of the microphone. According to [Moreau et al., 2006], the maximum aliasing-free operational frequency of a spherical microphone array is given by:

$$f_{max} = \frac{c}{2R\gamma}, \quad (2.11)$$

with c being the sound speed, and γ the maximum aperture angle between two capsules. It is important to notice the existence of a practical minimum frequency of the spherical microphone array, given by the low magnitude in low frequencies of high ambisonic order components, as shown in Fig. 2.2.

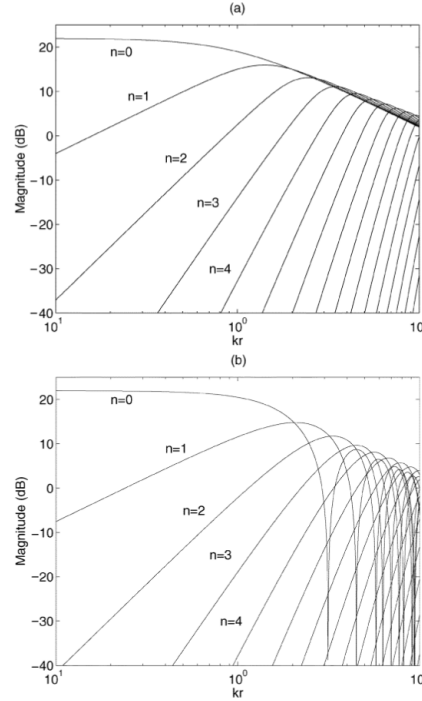


Figure 2.2: Magnitude of $\Gamma_n(kR)$ for different ambisonic orders, in the case of (a) rigid sphere, and (b) open sphere configurations. Adapted from [Rafaely, 2004].

2.3 Ambisonics

2.3.1 Ambisonics Theory

Ambisonics is a spatial sound recording and playback technology initially developed during the 1970s [Gerzon, 1973], and further expanded into its modern formulation around the 2000s [Daniel, 2000]. Ambisonics is based on the idea of decomposing a sound field into its spherical harmonic representation.

Originally, the decomposition was limited to first-order spheri-

cal harmonics, as the so-called *First Order Ambisonics* (FOA); mainly because of practical limitations. The technique was later formalized for arbitrary spherical harmonic orders, known as *Higher Order Ambisonics* (HOA). In general, with the term *ambisonics* we will be referring to the latter definition.

Ambisonic encoding

Let us consider a sound field composed of a point sound source S located in far-field at the angular position Ω_s . The sound pressure at the coordinate origin P can be expressed in terms of the spherical harmonic expansion of order N as: **check equation, find references, how to explain the domain? extend also to multiple sources by superposition**

$$P = \sum_{n=0}^N \sum_{m=-n}^n Y_n^m(\Omega_s) S \quad (2.12)$$

The ordered set of values of all spherical harmonics up to order N , evaluated at the source position, is known as the *ambisonic coefficients*:

$$Y_n^m(\Omega_s) = [Y_0^0(\Omega_s), Y_1^{-1}(\Omega_s), \dots, Y_N^N(\Omega_s)] \quad (2.13)$$

Furthermore, the process of multiplying the signal S by the ambisonic coefficients is known in the literature as the *ambisonic encoding*. The resulting signal vector is usually referred to as the *ambisonic* (or *B-Format*) signal S_n^m :

$$S_n^m = Y_n^m(\Omega_s) S \quad (2.14)$$

Although the term *B-Format* was initially introduced as an alternative name for first-order ambisonic signals [gerzon, tesis de daniel], it is nowadays common to use it as a synonym of ambisonic signals, without any order restriction. We will use the latter acception in what follows.

Historically, the name *B-Format* was used as an opposite of *A-Format*, which describes the signals recorded by a tetrahedral microphone array [Gerzon, 1975a]. The tetrahedron is the simplest and most common form of spherical microphone arrays (indistinctly referred to as ambisonic microphones) with uniform capsule distribution. Again, the term *A-Format* is also currently employed for referring to the signals recorded by any spherical microphone array, regardless of the number or arrangement of capsules.

Likewise, the process of signal conversion from the spatial domain (microphone capsules) to the spherical harmonic domain (ambisonic signals), as in Eq. 2.9, is known as *A-B conversion*. A number of different approaches have been developed for this process, and the interested reader is referred to [Moreau et al., 2006] for more information.

In practice, there are two alternative ways to generate ambisonic signals. The first one is the *synthesis*, based on the direct application of ambisonics encoding (Eq. 2.12) to a monophonic signal. The second one is the *recording* with a spherical microphone array, followed by the aforementioned domain conversion.

Ambisonic Decoding

Conversely, the sound field reconstruction is performed by the *ambisonic decoding* operation. This process is equivalent to weight-and-sum beamforming in the spherical harmonic domain, and it is sometimes also referred to as the *virtual microphone* technique [Zotter and Frank, 2019].

Let us consider a loudspeaker located at the angular position Ω_p . In accordance with Eq. 2.12, the signal feed P is *decoded* from the ambisonic signal as:

$$P = \sum_{n=0}^N \sum_{m=-n}^n Y_n^m(\Omega_s) S Y_n^m(\Omega_\ell) \alpha_n \quad (2.15)$$

Table 2.2: Ambisonic decoding: standard values of α_n weightings. Adapted from [Daniel, 2000].

Decoding	N	n			
		0	1	2	3
<i>basic</i>	0	1			
	1	1	1		
	2	1	1	1	
	3	1	1	1	1
<i>max-rE</i>	0	0.577			
	1	0.775	0.4		
	2	0.861	0.612	0.305	
	3	0.906	0.732	0.501	0.246
<i>in-phase</i>	0	0.333			
	1	0.5	0.1		
	2	0.6	0.2	0.029	
	3	0.667	0.286	0.071	0.008

where α_n is a weighting factor which accounts for the beam directivity. There are several standard weightings used for different purposes; their values are shown in Table 2.2, and the first-order directive patterns are plotted in Figure 2.3.

The decoding equation 2.15 can be written in matrix form as:

$$P = S_n^m Y_n^m(\Omega_p)^T \alpha_n \quad (2.16)$$

where the superscript T represents the matrix transposition. This equation can be extended to the usual case of decoding to a loudspeaker array, comprised of L loudspeakers located at the positions $\Omega_L = [\Omega_{p_1}, \dots, \Omega_{p_L}]$. In such case, the loudspeaker feed

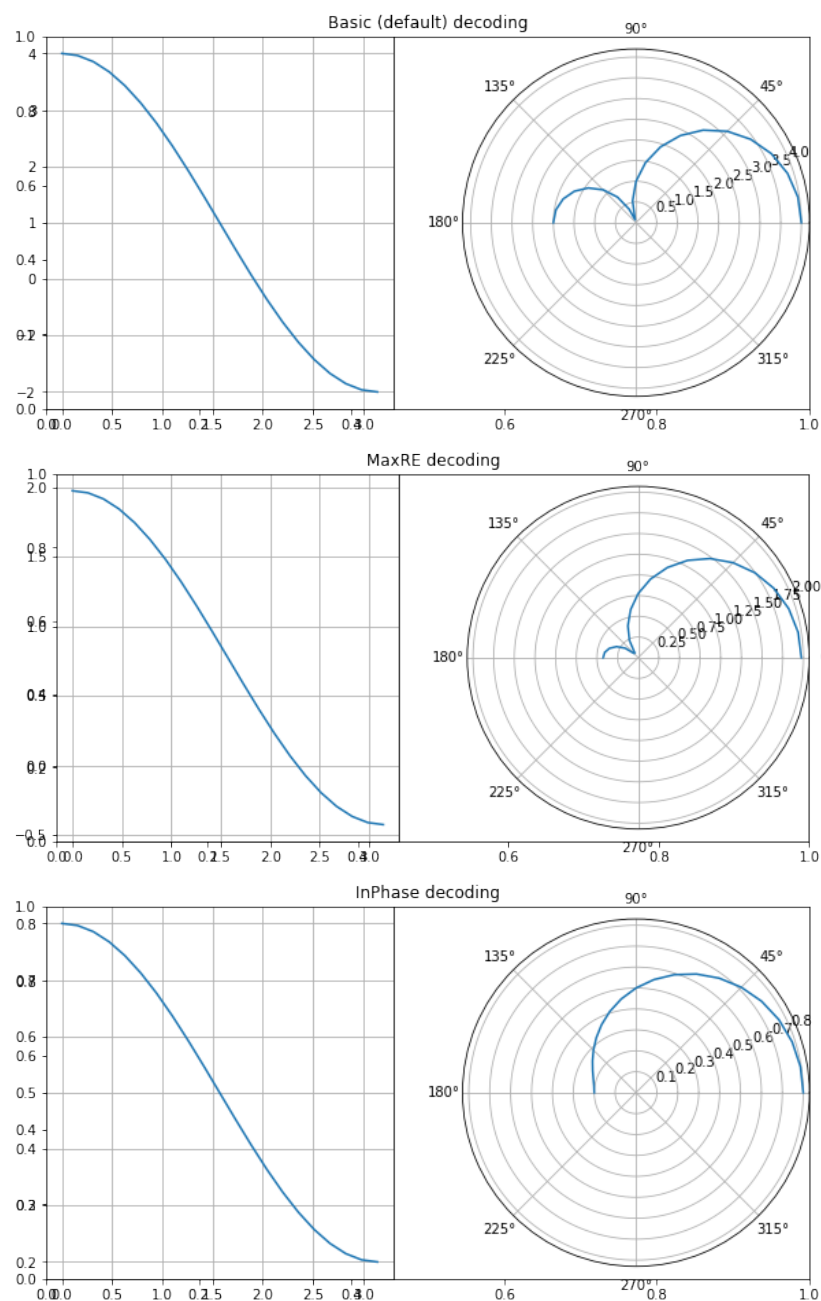


Figure 2.3: Directive patterns of first-order ambisonic decoding.

vector P_L can be written as:

$$P_L = S_n^m D, \quad (2.17)$$

where

$$D = \text{diag}(\alpha_n)[Y_n^m(\Omega_{p_1})^T, \dots, Y_n^m(\Omega_{p_L})^T] \quad (2.18)$$

is a $M \times L$ matrix known as the *decoding matrix*, and $\text{diag}(\alpha_n)$ is a diagonal matrix of size M containing the values of α_n along the main diagonal. Although the matrix D is frequency-independent and depends solely on the loudspeaker array geometry, in practical scenarios it is usual to include frequency-dependent weightings, $\alpha_n(k)$, to improve the broadband sound field reconstruction [Daniel, 2000].

Furthermore, sound field reconstruction with Eq. 2.17 is only possible when the loudspeakers are evenly located on the 3D space; in other words, the speaker layout must take the form of one of the five *Platonic solids*: tetrahedron, cube, octahedron, dodecahedron or icosahedron. Provided that this condition is usually difficult to fulfil in real scenarios, there are several methods which allow ambisonic decoding for such *irregular* layouts. One of the most commonly used is the AllRAD method [cite zotter](#). AllRAD proposes a two step decoding: first, the ambisonic signal is decoded to a nearly-uniform layout of virtual speakers. Then, the signals of the virtual speakers are further distributed into the real speakers by the *Vector-Based Amplitude Panning* (VBAP) method [cite pulkki](#).

2.3.2 Practical considerations

Due to historical and practical reasons, there are two aspects that must be taking into account when working with ambisonic signals: *channel normalization* and *channel ordering*. In the following, the term *channels* will be used as a synonym for spherical harmonics,

as they are usually referred to in sound engineering contexts¹.

Channel normalization

Let us consider the spherical harmonics $Y_n^m(\Omega)$ as defined in Eq. 2.3. Due to the orthonormal property showed in Eq. 2.7, they follow the *fully 3d normalized* or *N3D* channel normalization convention. **what about the $1/\sqrt{4\pi}$???**

Alternatively, the *Schmidt 3d semi-normalized* or *SN3D* [daniel] convention is also of widespread usage. The conversion between *N3D* and *SN3D* is driven by the following expression:

$$Y_n^m(\Omega)^{(N3D)} = \sqrt{2n+1} Y_n^m(\Omega)^{(SN3D)} \quad (2.19)$$

MaxN is another existing convention. It defines all spherical harmonics as having a maximum absolute value of 1:

$$\max_{\Omega} |Y_n^m(\Omega)^{(MaxN)}| = 1, \forall (n, m) \quad (2.20)$$

Finally, the *Furse-Malham* (or *FuMa*) normalization only differs from *Max-N* in the scaling of the zero-th order component:

$$Y_n^m(\Omega)^{(FuMa)} = \begin{cases} 1/\sqrt{2}, & \text{if } n = 0, \\ Y_n^m(\Omega)^{(MaxN)}, & \text{else.} \end{cases} \quad (2.21)$$

Each of the normalization schemes has its own particularities. For instance, *N3D* is the most mathematically straightforward, and spherical harmonics defined in that way can be directly used for both encoding and decoding (as in Eqs 2.12 and Eq. 2.15) – however, from a sound engineer point of view, other normalization schemes with maximum values below the unity might be preferred, such

¹In fact, ambisonic signals are inherently multichannel, even though each channel corresponds to a spherical harmonic, and not to a loudspeaker feed as in traditional *channel-based* audio.

as *SN3D*. Besides this, *FuMa* has been historically the default normalization [Gerzon, 1985], while the more modern *N3D* and *SN3D* were popularized after [Daniel, 2000].

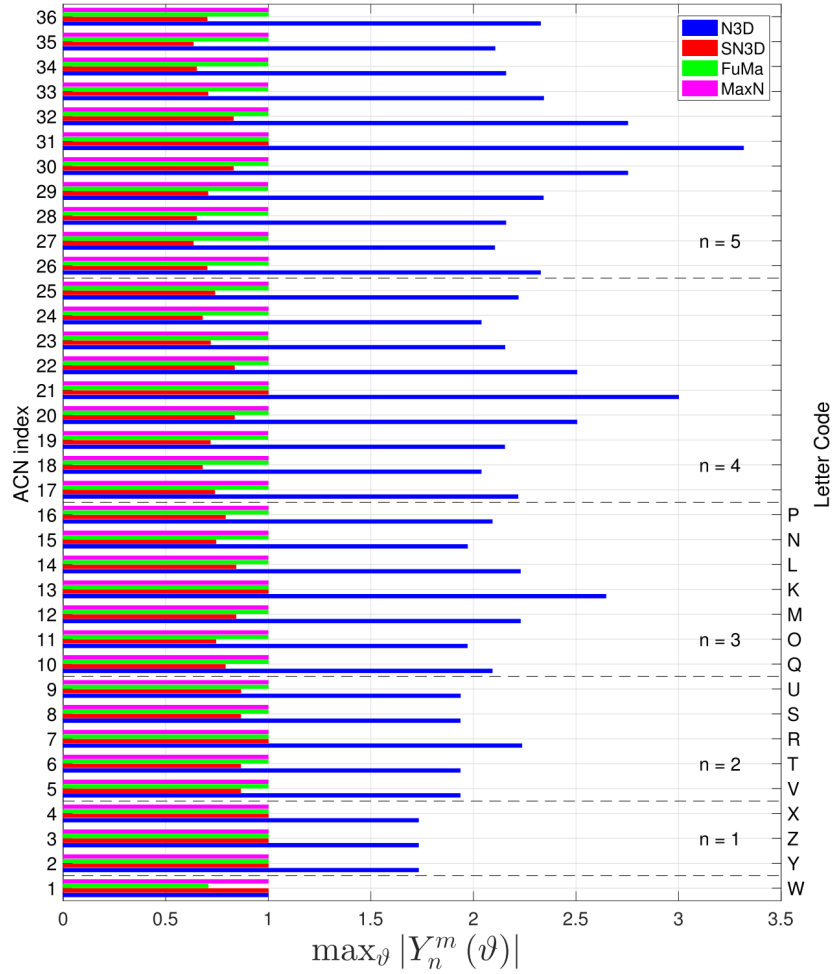


Figure 2.4: Maximum value of each ambisonic channel up to order 5, for all different normalization schemes. Image from [Carpentier, 2017].

As a summary, Figure 2.4 displays the different normalization schemes. The reader is referred to [Carpentier, 2017] for an extensive review on the topic.

Channel ordering

Channel ordering refers to the manner in which spherical harmonics, inherently organized in the 2D space by dimensions n and m , are sorted into a one-dimensional vector.

The ACN (from *Ambisonic Channel Number*) scheme follows from the mathematical description given in Eq. 2.13. The spherical harmonics are first ordered by ascending order n and, inside each order, by ascending degree m . The index of a given channel $i \in [0 \dots M-1]$ can be thus obtained by the following relationship:

$$i = n^2 + n + m \quad (2.22)$$

Historically, first-order ambisonic audio has followed what it might be called *traditional B-Format* channel ordering [Gerzon, 1985]. By this scheme, the four channels of a FOA signal S_n^m are referred to by the axis where the corresponding spherical harmonic steers, plus the name W for the zeroth order component:

$$S_n^m(\Omega)^{(\text{FuMa CO})} = [W, X, Y, Z] \quad (2.23)$$

where:

$$\begin{aligned} W &= S_0^0(\Omega) \\ X &= S_1^1(\Omega) \\ Y &= S_1^{-1}(\Omega) \\ Z &= S_1^0(\Omega) \end{aligned} \quad (2.24)$$

This nomenclature was extended to second and third order, and is currently known as the *Furse-Malham* or *FuMa* channel ordering. The channel names use all english alphabet letters from K to Z in third order and, although there would be enough letters to go up

to fourth order, the inconvenience of the system was clear [Malaham, 2003]. Figure 2.4 shows the equivalence between *FuMa* (“letter code”) and *ACN* channel names.

In practice, there exist two main combinations of channel normalization and ordering schemes:

- The *classical* approach, usually limited to first-order ambisonics, which uses *FuMa* normalization and channel ordering².
- The *modern* approach, inspired by the *ambix* file format [cite ambix], with *SN3D* normalization and *ACN* channel ordering.

Anyhow, the *classical B-Format* channel naming and ordering is still widely used when referring to first-order ambisonics.

2.4 Parametric Spatial Audio Analysis

Trough parametric analysis, sound fields may be described in terms of a small amount of sound sources and associate parameters. Such representation might reduce to a great extent the complexity of processing methods [Jarrett et al., 2017].

One of the most successful sound field parametric models is *DirAC* [Pulkki, 2007], which was originally conceived as a method for impulse response processing and spatial sound reproduction [Merimaa and Pulkki, 2005].

DirAC (acronym for *Directional Audio Coding*) is a perceptually motivated time-frequency (TF) domain method, based on the assumption that any sound field may be reproduced with high perceptual quality by considering two parameters: the sound field diffuseness and the most prominent sound *Direction-of-Arrival* (DOA) [Pulkki et al., 2018].

²In general, it may be expected that *early* ambisonic material follow these conventions without any explicit mention to them.

Let us consider a *SN3D*-normalized first-order ambisonic signal in time-frequency domain, $S_n^m(k, n)$. For the sake of clarity, we will use in this section *FuMa* channel notation and ordering (Eq. 2.23):

$$S_n^m(k, n) = [W(k, n), X(k, n), Y(k, n), Z(k, n)] \quad (2.25)$$

Given this representation, we can express the *pressure* $P(k, n)$ of the sound field as:

$$P(k, n) = W(k, n) \quad (2.26)$$

as well as the sound *pressure-gradient* (or *velocity*) $\mathbf{U}(k, n)$ as:

$$\mathbf{U}(k, n) = -\frac{1}{\rho_0 c} [X(k, n), Y(k, n), Z(k, n)], \quad (2.27)$$

where ρ_0 is the mean density of the medium, and c is the speed of sound.

The *active intensity* $\mathbf{I}(k, n)$, defined as the amount of transmitted acoustic energy, can be expressed in terms of sound pressure and velocity [Fahy and Salmon, 1990]:

$$\begin{aligned} \mathbf{I}(k, n) &= \Re\{P^*(k, n)\mathbf{U}(k, n)\} \\ &= -\frac{1}{\rho_0 c} \Re\{W^*(k, n)[X(k, n), Y(k, n), Z(k, n)]\}, \end{aligned} \quad (2.28)$$

where $*$ represents the complex conjugate operator.

An estimate of the instantaneous DOA $\Omega(k, n)$ can be extracted from the intensity vector, interpreting each of its time-frequency bins as a point in the cartesian space. Effectively, the sound propagation direction is the opposite to the observed arrival direction.

$$\Omega(k, n) = \angle(-\mathbf{I}(k, n)), \quad (2.29)$$

with \angle representing the spherical angle operator of a cartesian vector. The result of this computation must be understood as the

direction of the net energy flow, which in the case of a single plane-wave will correspond to the source position.

Another useful parameter is the *energy density* $E(k, n)$ [Stanzial et al., 1996]:

$$\begin{aligned} E(k, n) &= \frac{1}{2\rho_0 c^2} |P(k, n)|^2 + \frac{1}{2} \|\mathbf{U}(k, n)\|^2 \\ &= \frac{1}{2\rho_0 c^2} \left(|W(k, n)|^2 + \|[X(k, n), Y(k, n), Z(k, n)]\|^2 \right). \end{aligned} \quad (2.30)$$

Finally, the *diffuseness* $\Psi(k, n)$ can be computed from the sound intensity and energy density [Merimaa and Pulkki, 2005]:

$$\begin{aligned} \Psi(k, n) &= 1 - \frac{\|\langle \mathbf{I}(k, n) \rangle\|}{c \langle E(k, n) \rangle} \\ &= 1 - 2 \frac{\|\langle \Re\{W^*(k, n)[X(k, n), Y(k, n), Z(k, n)]\} \rangle\|}{\langle |W(k, n)|^2 + \|[X(k, n), Y(k, n), Z(k, n)]\|^2 \rangle}, \end{aligned} \quad (2.31)$$

where the symbols $\langle \cdot \rangle$ represent the expectation operator, which is usually implemented as time-domain averaging.

Even though Eq. 2.31 (known as *DirAC’s diffuseness*) is one of the most common ambisonic diffuseness estimators, several alternative formulations exist. Other diffuseness estimation procedures include the *coefficient of variation method* [Ahonen and Pulkki, 2009] and the more recent *COMEDIE* estimator [Epain and Jin, 2016]. In any case, in what follows, the term *diffuseness* and the symbol Ψ will refer by default to Eq. 2.31.

As a mathematical convenience, we will define the *B-Format coherence* as the complement of the diffuseness:

$$\Delta(k, n) = 1 - \Psi(k, n) \quad (2.32)$$

In conclusion, Figure 2.5 plots the spectrograms of the DOA $\Omega(k, n)$ and diffuseness $\Psi(k, n)$ of a FOA recording, which consists

of a sound source located at the front, plus a moderate amount of reverberation and background noise.

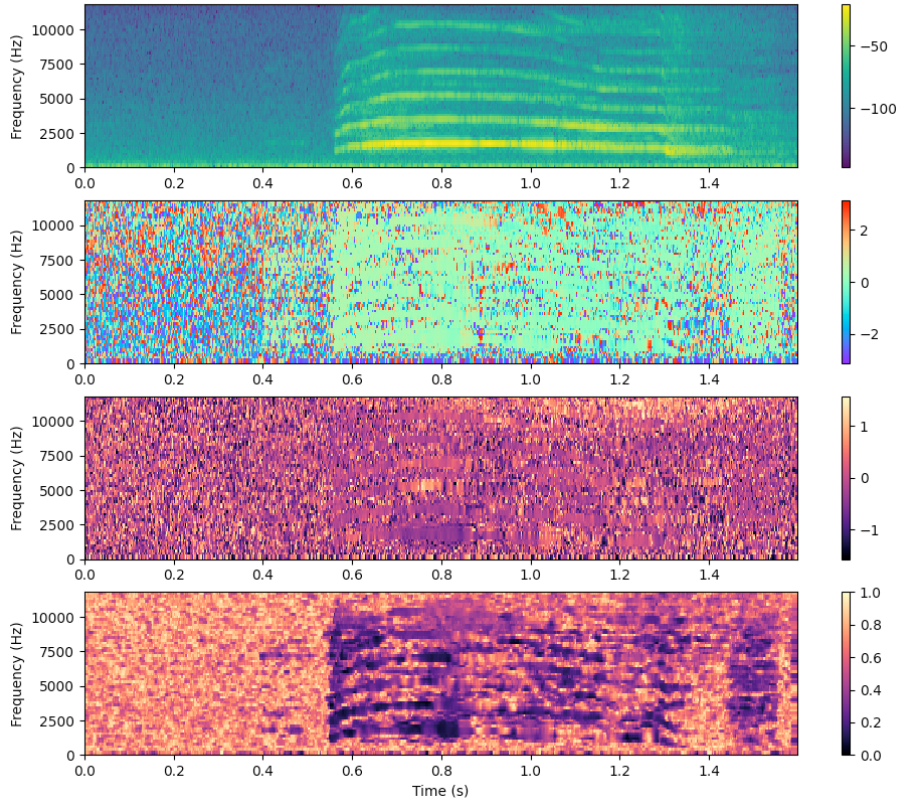


Figure 2.5: Parametric time-frequency spatial audio analysis of a first order ambisonic recording. From top to bottom: 1.) Magnitude spectrogram of the omnidirectional channel. 2.) and 3.) Azimuth and elevation of the estimated instantaneous narrowband DOAs $\Omega(k, n)$. 4.) Instantaneous narrowband diffuseness $\Psi(k, n)$.

2.5 Spatial Coherence Analysis

put this chapter in context or something

In the context of microphone array signal processing, diffuseness is commonly estimated through the *Magnitude Squared Coherence* (MSC) [Elko, 2001] between two frequency-domain signals S_1 and S_2 , as a function of the *wavenumber* k and the microphone distance r :

$$\text{MSC}_{12}(kr) = \frac{|\langle S_1(kr)S_2(kr)^* \rangle|^2}{\langle |S_1(kr)|^2 \rangle \langle |S_2(kr)|^2 \rangle}, \quad (2.33)$$

where the $\langle \cdot \rangle$ operator represents the temporal expected value, and $*$ defines the complex conjugate operator. In the case of spherical isotropic noise fields, Eq. (2.33) can be expressed in terms of microphone directivity patterns $T(\phi, \theta, kr)$ as [Elko, 2001]:

$$\begin{aligned} \text{MSC}_{12}(kr) &= \frac{|N_{12}(kr)|^2}{|D_{12}(kr)|^2} \\ &= \frac{|\int_0^\pi \int_0^{2\pi} T_1(\phi, \theta, kr)T_2^*(\phi, \theta, kr)e^{-jkr\cos\theta}\sin\theta d\theta d\phi|^2}{|\sqrt{\int_0^\pi \int_0^{2\pi} |T_1(\phi, \theta, kr)|^2 \sin\theta d\theta d\phi} \sqrt{\int_0^\pi \int_0^{2\pi} |T_2(\phi, \theta, kr)|^2 \sin\theta d\theta d\phi}|^2}. \end{aligned} \quad (2.34)$$

Moreover, the general expression of the directivity of a first-order differential microphone is given by the following relationship:

$$T_i(\Omega_i) = \alpha_i + (1 - \alpha_i) \cos \Omega_i, \quad (2.35)$$

where $i \in [1, 2]$ is the microphone index, Ω_i is the angle between wave incidence and microphone orientation axis, and $\alpha_i \in [0, 1]$ is the directivity parameter of the microphone i , which ranges from bidirectional ($\alpha_i = 0$) to omnidirectional ($\alpha_i = 1$).

For first-order differential microphones, there is a closed-form expression for the numerator and denominator of Eq. (2.34):

$$\begin{aligned}
 N_{12}(kr) &= \frac{\alpha_1 \alpha_2 \sin(kr)}{kr} \\
 &+ \frac{(1 - \alpha_2)(1 - \alpha_2)(x_1 x_2 + y_1 y_2)}{(kr)^3} (\sin(kr) - kr \cos(kr)) \\
 &+ \frac{z_1 z_2}{kr^3} [((kr)^2 \sin(kr) + 2kr \cos(kr))(1 - \alpha_1)(1 - \alpha_2) + 2\sin(kr)(1 - \alpha_1)(1 - \alpha_2)] \\
 &+ \frac{z_1}{(kr)^3} [j(kr)^2 \alpha_2 \cos(kr)(\alpha_1 - 1) + jkr \alpha_2 \sin(kr)(1 + \alpha_1)] \\
 &+ \frac{z_2}{(kr)^3} [j(kr)^2 \alpha_1 \cos(kr)(\alpha_2 - 1) + jkr \alpha_1 \sin(kr)(1 + \alpha_2)], \\
 D_{12}(kr) &= \frac{\sqrt{3\alpha_1^2 + (1 - \alpha_1)^2} \sqrt{3\alpha_2^2 + (1 - \alpha_2)^2}}{3},
 \end{aligned} \tag{2.36}$$

where x_i , y_i and z_i are the cartesian coordinates of the wave incidence angle Ω_i . **check**.

2.6 Reverberation

In the context of room acoustics, reverberation refers to “the energy of a sound source that reaches a listener indirectly, by reflecting from surfaces within the surrounding space occupied by the sound source and the listener” [Begault and Trejo, 2000]. Conversely, in anechoic or free-field conditions, where reverberation is not present, only the direct path of the sound source exists. Assuming linearity and time-invariance, room reverberation can be fully characterised by its impulse response (IR).

Reverberation models often consider two differentiated parts of the reverberant tail, based on both physical and perceptual characteristics: the *early reflections* and the *late reverberation*. Early reflections, as the name suggests, refers to the individual sound paths

arriving to the listener after a few reflections on the room surfaces, which cause some degree of attenuation. Early reflections typically arrive with a time difference between 1 and 80 ms after the direct path [Begault and Trejo, 2000]. The term late reverberation encompasses all sound paths arriving to the listener after many reflections. Since the temporal density of such reflections increases with time, late reverberation is often modelled in statistical terms. An schematic representation of a room impulse response (RIR) is shown in Figure 2.6.

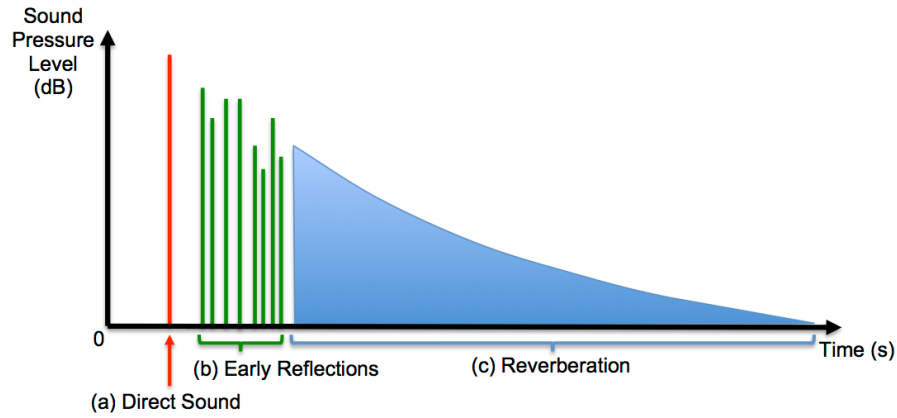


Figure 2.6: Room impulse response model, from [Murphy et al., 2017].

By following this model, a RIR $h(t)$ can be described as a sequential combination of responses:

$$h(t) = h_D(t) + h_R(t), \quad (2.37)$$

where $h_D(t)$ and $h_R(t)$ represent the *direct* (direct path plus early reflections) and *reverberant* (late reverberation) components of the

RIR. respectively.

The room impulse response is a function of both the source and the receiver locations. Different levels, delays and directions of direct path and early reflections can be obtained from measurements in the same room. However, it is generally assumed that the late reverberation is fixed for a given room, regardless of source/receiver positions.

Room reverberation plays an important role in psychoacoustics. While early reflections are usually perceived together with the direct path as a single auditory event, due to the *precedence effect* [Haas, 1972], late reverberation has often an influence on the received signal. In the specific case of speech, late reverberation is associated with a loss of intelligibility [Braun, 2018]. In the context of spatial perception, it has been shown that early reflections help the localization and externalization of sources [Rudrich and Frank, 2019], while the late reverberation is associated with a spaciousness perception of the room [Begault and Trejo, 2000].

There are a number of measurable parameters which help to characterise room acoustics. Perhaps one of the most widespread is the *reverberation time* T_{60} [Kuttruff, 2016]. It represents the time required for the reverberant sound field power to decay by 60 dB. Reverberation time can be accurately computed from the room geometry [Sabine, 1927] or from the IR [Schroeder, 1965].

In the latter case, the T_{60} value is usually estimated from the *Energy Decay Curve* (EDC), which is defined as:

$$\text{EDC}(t) = 10 \log_{10} \sum_{t'=t}^{\infty} h^2(t'), \quad (2.38)$$

where $h(t)$ represents the room impulse response. The values are normalized such that the maximum peak of the curve corresponds to 0 dB.

Table 2.3: Reverberation time computation: usual reference levels

	EDT	T_{10}	T_{20}	T_{30}
$L_{max}(dB)$	0	-5	-5	-5
$L_{min}(dB)$	-10	-15	-25	-35

The EDC is usually modelled as a straight line in logarithmic scale. Therefore, the T_{60} estimation is performed by estimating the slope of a straight line between two reference levels on the EDC time series. Some of the most used reference levels receive specific names: *Early Decay Time* (EDT), T_{60} , and reverberation times T_{10} , T_{20} and T_{30} . Table 2.3 shows their correspondent reference levels, where the maximum energy peak is normalized to 0 dB. An schematic representation of the reference levels is depicted in Figure 2.7.

An alternative parameter is the *decay rate* α_{60} , which is related to reverberation time T_{60} as:

$$\alpha_{60} = \frac{3 \ln(10)}{T_{60}} (\text{dB/s}). \quad (2.39)$$

The decay rate is thus the slope of the EDC curve, in logarithmic scale, expressed in dB per second.

To conclude, it is important to notice that reverberation time is frequency-dependent. Accordingly, it is usual to report it for octave or third-octave bands, or alternatively to provide its value at a specific frequency.

The *Direct to Reverberant Ratio* (DRR) is another relevant acoustic parameter. DRR represents the ratio between direct and reverberant parts of the RIR, as defined in Eq. 2.37:

$$DRR = 10 \log_{10} \frac{\sum_{t=1}^{L_D} h_D^2(t)}{\sum_{t=1}^{L_R} h_R^2(t)}, \quad (2.40)$$

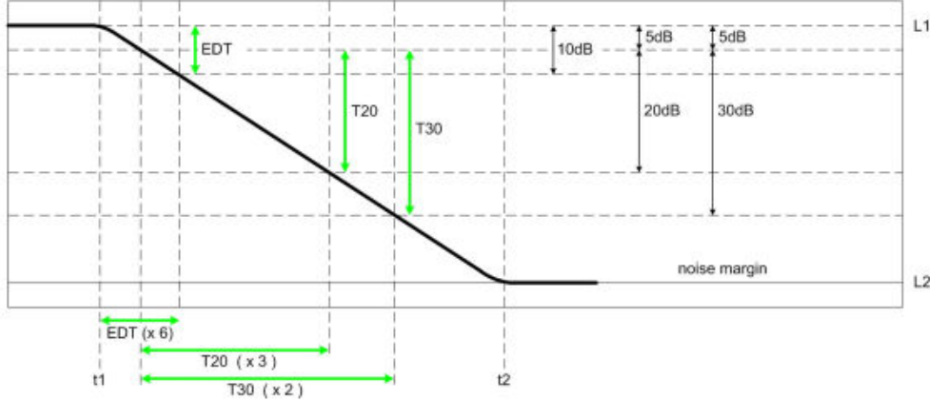


Figure 2.7: Room impulse response model, adapted from <http://www.bnoack.com/>.

with L_D and L_R as the length of the direct $h_D(t)$ and reverberant $h_R(t)$ filters, respectively. At a psychoacoustic level, the direct to reverberant ratio is one of the main cues for distance perception [Begault and Trejo, 2000].

Since the direct path and early reflections (but not the late reverberation) depend on the relative position between source and receiver, the filter $h_D(t)$ and therefore the DRR are as well location-dependent. For a given room, the source-receiver distance that produces a DRR of 0 dB is known as the *critical distance*.

RIR SIMULATION: IMAGE METHOD

2.7 Signal Models

Let us consider a sound source represented by the signal $s(t)$, located in a given acoustic enclosure characterised by its room impulse response $h(t)$. The resulting reverberant signal $x(t)$ can be therefore described as the *convolutive mixture* of the source and the

RIR:

$$x(t) = s(t) * h(t). \quad (2.41)$$

When dealing with multichannel room impulse responses, as it is the case in ambisonics, the multichannel reverberant signal $x_m(t)$ is obtained by the convolutive mixture of each RIR channel independently:

$$x_m(t) = s(t) * h_m(t). \quad (2.42)$$

The time domain convolution operation, under certain assumptions, is equivalent to the multiplication in frequency domain. By doing so, Eq. 2.41 can be expressed as:

$$X(k, n) = S(k, n)H(k, n). \quad (2.43)$$

Eq. 2.43, also known as the *Multiplicative Transfer Function (MTF) model* is only valid when the length of the filter $h(t)$ is smaller than the length of the analysis window used in the STFT.

On the contrary, when the filter $h(t)$ spans across several analysis windows, the resulting model is referred to as the *Convolutional Transfer Function (CTF) model*:

$$X(k, n) = \sum_{l=0}^{L_h-1} H(k, l)S(k, n-l), \quad (2.44)$$

where L_h is the length of the filter $H(k, n)$ in time frames.

isotropic noise

Chapter 3

Blind reverberation time estimation

3.1 Introduction

Knowledge about the acoustic properties of an enclosure is a fundamental topic with many applications in the microphone array and acoustic signal processing field. Problems such as dereverberation [Braun et al., 2018] or source separation [Gannot et al., 2017] may benefit from this information, and may require prior estimation of the related parameters.

The 2016 Acoustic Characterisation of Environments (ACE) Challenge [Eaton et al., 2016] gathered dozens of methods designed for blind T_{60} and Direct-to-Reverberation Ratio (DRR) estimation; nowadays, it is still considered as a state-of-the-art source for performance evaluation and comparison among methods.

Most of the model-based T_{60} estimation algorithms consider the reverberant signal envelope as an exponential decay, so that the problem is reduced to finding a signal offset and estimate the decay rate. Moreover, in last years, data-driven models have outperformed the previous state-of-the-art results [Gamper and Tashiev, 2018, Looney and Gaubitch, 2020, Bryan, 2020]. A compara-

tive review on single-channel blind T_{60} estimation algorithms was recently published [Löllmann et al., 2019].

However, most of the existing reverberation time estimation methods focus on the single-channel case. A representative example can be drawn from the ACE Challenge, where, despite the fact that one of the reverberant datasets was recorded with an *em32 Eigenmike* spherical microphone array, none of the methods use of it for the T_{60} estimation task.

On the other hand, recent years have witnessed a growing interest in immersive audio for virtual and augmented reality. This situation has consolidated Ambisonics [Zotter and Frank, 2019] as the *de facto* standard for spatial audio. Dedicated spherical microphone arrays have reached the market in last years; their multichannel nature makes possible spatial manipulations that complement traditional signal enhancement methods.

In this chapter, we present a novel approach to the problem of multichannel blind reverberation time estimation, specifically focusing on first order ambisonic (FOA) recordings. The method is based on a dereverberation stage followed by system identification. To the best of our knowledge, the proposed algorithm is the first reverberation time estimation method specifically designed for first order ambisonic audio.

The rest of the chapter is organized as follows. Section 3.2 introduces the nomenclature and the signal model. Sections 3.3 and 3.4 describe the baseline and the proposed methods, respectively. The experimental setup is described in Section 3.5, and the results are discussed in Section 5.5. Finally, a conclusion is presented in Section 3.7.

3.2 Signal Model

Let us consider a FOA signal $x_n^m(t)$, with $M = 4$ as the number of channels. Let us further assume the convolutive mixture signal

model described in Eq. 2.42, where the reverberant signal $x_n^m(t)$ represents the signal captured by an ideal spherical microphone array located in a reverberant enclosure. Let $s(t)$ denote the signal of the only sound source present in the scene, and $h_n^m(t)$ denote the ambisonic RIR modelling the acoustic enclosure:

$$x_n^m(t) = s(t) * h_n^m(t) \quad (3.1)$$

It is important to remark that T_{60} estimation here assumes no receiver directionality. In an ambisonic context, this corresponds to the zeroth order component. Therefore, in what follows, all methods estimating IR parameters will be applied to the zeroth order channel, $x_0(t)$.

3.3 Baseline method

The baseline algorithm, taken from [Prego et al., 2012], is based on the detection of abrupt event offsets in the time-frequency domain. The subband energy decay on the transitions can be then used to compute an estimate of the full-band decay. This method performed best in the ACE Challenge regarding the Pearson correlation coefficient between estimated and true T_{60} [Eaton et al., 2016].

Let us consider the zeroth order channel of the recorded signal, $x_0(t)$, and its Short-Time Frequency Transform (STFT) counterpart $X_0(k, n)$. The *subband energy* $\bar{E}(k, n)$ of the recorded signal can be expressed as:

$$\bar{E}(k, n) = |X_0(k, n)|^2. \quad (3.2)$$

A *Free Decay Region* (FDR) is defined as a group of consecutive bins within the same subband which exhibit a monotonically decreasing energy. A FDR search is performed on the subband energy spectrogram $\bar{E}(k, n)$: for each band, the algorithm tries to find at least one FDR, iteratively reducing the FDR length if no candidates are found.

The next step is the estimation of the reverberation time, which is performed using a subband equivalent of Schroeder’s method [Schroeder, 1965]. The *Subband Energy Decay Function* (SEDF) associated with a given FDR is computed as:

$$\bar{c}(k, n) = 10 \log_{10} \frac{\sum_{\nu=n}^{L_c-1} \bar{E}(k, \nu)}{\sum_{\nu=0}^{L_c-1} \bar{E}(k, \nu)} \text{dB}, \quad (3.3)$$

where $n = 0 \dots, L_c - 1$ spans the length of the FDR. A linear regression is then performed on each SEDF curve: T_{60} is computed as the time required by the resulting line to reach the -60 dB reference.

This procedure yields a T_{60} estimate per FDR. In order to obtain a global estimate, the algorithm proposes a two-step statistical filtering. First, it obtains a narrowband estimate as the median of all estimates within each subband. Then, the resulting broadband value \bar{T}_{60} is computed as the median of all subband estimates. The last step of the method is the expansion of the resulting dynamic range by a linear mapping. This procedure is required because of the compression introduced by the median operator. The final value T_{60} is thus a linear mapping of \bar{T}_{60} , where the parameters α and β might be obtained by linear regression on a training stage:

$$T_{60} = \alpha \bar{T}_{60} + \beta \quad (3.4)$$

3.4 Proposed method

We propose a novel method for reverberation time estimation, based on two steps: signal dereverberation, and system identification. The main idea consist in obtaining an estimate of the dereverberated signal, which is later used for estimating the multichannel IR given the recorded reverberant signal. The reverberation time can be thus computed by the decay slope of the estimated IR.

3.4.1 Dereverberation

Let us consider now the *CTF* model (Eq. 2.44) version of the proposed signal model:

$$X_m(k, n) = \sum_{l=0}^{L_h-1} H_m(k, l) S(k, n - l), \quad (3.5)$$

where the multichannel filter $H_m(k, l)$ of length L_h contains the *CTF coefficients* between the source and the microphones.

Considering the room impulse response model of Eq. 2.37, it is possible to sequentially split the former expression in the following way:

$$\begin{aligned} X_m(k, n) &= D_m(k, n) + R_m(k, n) = \\ &= \sum_{l=0}^{\tau-1} H_m(k, l) S(k, n - l) + \sum_{l=\tau}^{L_h-1} H_m(k, l) S(k, n - l), \end{aligned} \quad (3.6)$$

where the parameter τ represents the *mixing time*, which states the transition time between early reflections and late reverberation. In other words, the captured signal is divided between a *direct* part $D_m(k, n)$, containing the direct path and the early reflections, and a *reverberant* part $R_m(k, n)$, which mainly contains the diffuse part of the reverberation.

Assuming a Multichannel Auto-Regressive (MAR) model, $R_m(k, n)$ can be expressed as a multichannel Infinite Impulse Response (IIR) filter applied to the recorded signal:

$$R_m(k, n) = \sum_{i=1}^M \sum_{l=0}^{L_g-1} X_i(k, n - \tau - l) G_{mi}(k, l), \quad (3.7)$$

where the coefficients $G_{mi}(k, l) \in \mathbb{C}$ model the relation between channels m and i , and have a length of L_g frames.

By grouping all time frames $n = 1 \dots, N - 1$, it is possible to express Eq. 3.7 in vector notation:

$$\mathbf{R}_m(k) = \tilde{\mathbf{X}}_\tau(k) \mathbf{G}_m(k), \quad (3.8a)$$

$$\tilde{\mathbf{X}}_\tau(k) = [\tilde{\mathbf{X}}_{\tau,1}(k), \dots, \tilde{\mathbf{X}}_{\tau,M}(k)], \quad (3.8b)$$

where $\tilde{\mathbf{X}}_{\tau,m}(k)$ is a $N \times L_g$ matrix, and $\mathbf{R}_m(k)$ and $\mathbf{G}_m(k)$ are column vectors with lengths N and $L_g M$, respectively.

Finally, the expression can be further simplified by omitting the frequency dependence, and by expressing the channels as columns in the vector notation. Substituting this expression in Eq. 3.6 leads to the MAR equation:

$$\mathbf{D} = \mathbf{X} - \tilde{\mathbf{X}}_\tau \mathbf{G}. \quad (3.9)$$

Here, the dereverberation problem consists in the estimation of the MIMO filter \mathbf{G} , so that the *clean* signal \mathbf{D} (containing both direct path and early reflections) can be computed.

The algorithm proposed here is based on the method described in [Jukić et al., 2015]. In this case, the dereverberation problem is tackled as an optimization problem, considering that the spectrograms of the reverberant signal are less sparse than those of the corresponding *clean*, and ensuring that the inter-channel signal properties are maintained. Although the presented method is applied on the whole signal in *batch* mode, alternative *online* methods could be also used, e.g. [Braun and Habets, 2016].

By using *iteratively reweighted least squares* (IRSL) [Chartrand and Yin, 2008], it can be shown that an iterative solution for the estimation of \mathbf{G} at the iteration (i) is given by the following expression:

$$\mathbf{G}^{(i)} = (\tilde{\mathbf{X}}_\tau^H \mathbf{W}^{(i)} \tilde{\mathbf{X}}_\tau)^{-1} \tilde{\mathbf{X}}_\tau^H \mathbf{W}^{(i)} \mathbf{X}, \quad (3.10)$$

where $\mathbf{W}^{(i)}$ is a $N \times N$ diagonal matrix whose diagonal values, $w_n^{(i)}$, can be updated as:

$$w_n^{(i)} = (\mathbf{d}_n^{H(i-1)} \Phi^{-1(i-1)} \mathbf{d}_n^{(i-1)})^{\frac{p-2}{2}} + \epsilon. \quad (3.11)$$

In turn, \mathbf{d}_n represents the rows of \mathbf{D} arranged as column vectors of length M , Φ is the $M \times M$ Spatial Covariance Matrix (SCM) of \mathbf{D} , ϵ is an arbitrary small positive value, and $p \leq 1$. The computation and update of the SCM matrix is given by:

$$\Phi^{(i)} = \frac{1}{N} \mathbf{D}^{T(i)} \mathbf{W}^{(i)} \mathbf{D}^{*(i)}. \quad (3.12)$$

To conclude the dereverberation method, Eqs. 3.9, 3.10, 3.11 and 3.12 can be applied iteratively, starting by updating Eq. 3.11, until convergence is reached:

$$\|\mathbf{D}^{(i)} - \mathbf{D}^{(i-1)}\|_F / \|\mathbf{D}^{(i)}\|_F < \eta, \quad (3.13)$$

where η is an arbitrary small positive value, or alternatively until the maximum number of iterations i_{max} is exceeded. For the initialization, the following values are proposed: $\mathbf{D} = \mathbf{X}$ and $\Phi = \mathbf{I}_M$ (the identity matrix of size $M \times M$).

3.4.2 System Identification

The output of the dereverberation step is the multichannel signal D_m , which ideally contains the direct plus early reflection components of the source. Therefore, given the reverberant signal X_m and the dereverberated signal D_m , an estimate of the late room impulse response might be derived by identifying the filter connecting the two. As stated in Section 3.2, we are primarily interested on the response of the omnidirectional channel; for that reason, the filter estimation is performed with the zeroth order components of both recorded and dereverberated signals. We perform system identification directly in the STFT through a linear fit between input and output independently for every frequency bin:

$$\hat{H}_0(k) = \frac{\mathbf{d}_0^H(k) \mathbf{x}_0(k)}{\mathbf{d}_0^H(k) \mathbf{d}_0(k)}, \quad (3.14)$$

where $\mathbf{d}_0, \mathbf{x}_0$ are $N \times 1$ length vectors. To avoid complex cross-band modeling of the system response, we use a long STFT window, assumed longer than the twice the length of the IR so that a reduction of the CTF to a Multiplicative Transfer Function (MTF) holds [Avargel and Cohen, 2007].

As a last step, the estimated time-frequency filter $\hat{H}_0(k, n)$ is transformed into the time domain filter $\hat{h}(t)$. The T_{60} is then computed by linear fitting of the Schroeder integral in the $[-5, -15]$ dB range (T_{10} estimation method), after filtering $\hat{h}(t)$ with an octave-band filter centered at 1 kHz.

3.5 Experimental setup

3.5.1 Dataset

The proposed method is evaluated using two different reverberant datasets, containing recordings of *speech* and *drums* respectively. In order to have full control over the reverberation conditions in the experimental setup, the audio clips under consideration have been rendered by the convolutive mixture of clean monophonic recordings with FOA IRs.

The *speech* dataset is composed of the LibriSpeech [Panayotov et al., 2015] *test-clean* audio samples longer than 25 s, making a total of 30 audio clips. It contains English language sentences by male and female speakers, often with a small level of background noise. We have used only a 20 s long excerpt of each clip, preceded by an initial offset of 5 s. The *drums* dataset is the *test* subset of the isolated drum recordings from the DSD100 dataset [Liutkus et al., 2017]. It contains 50 different audio clips, covering a wide range of music and mixing styles. The same audio lengths and offsets as in the previous case are applied.

The IRs are FOA room impulse responses simulated by the image method with the *Multichannel Acoustic Signal Processing* library [ref to chapter?]. There are 9 different IRs of 1 s, with random T_{60}

values in the range between 0.4 s and 1.1 s approximately, estimated by the T_{10} method at the 1 kHz band. The angular position of the sources is randomized for each IR, while the receiver position is fixed at the room center, which has a size of $10.2 \times 7.1 \times 3.2$ m. The source distance is set to half the *critical distance*, thus providing positive DRRs.

The combination of the dry audio clips with the IRs yields a total of 270 and 450 audio clips for the *speech* and *drums* datasets, respectively, after removing the audio clips which mostly contain silence. Those datasets will be referred in the following as the *evaluation* datasets.

Finally, the baseline method requires a previous *fitting* step for the computation of the mapping parameters α and β from Eq. 3.4. The procedure has been performed as follows. For the *speech* dataset, we selected again the subset of audio clips longer than 25 s, but in this case on the *dev-clean* dataset, which yields a total of 20 audio clips. For the *drums* dataset, we used the 50 clips of the *development* subset. The generation of the convolutive mixes has followed the same procedure as in the previous case. We will refer to the resulting datasets as the *development* datasets.

3.5.2 Setup

The sampling frequency for all methods is 8 kHz. For the baseline system, the window size is 1024 samples long, with an overlap of 256 samples. The FDR length is set to 500 ms, which has been reported as the ideal theoretical minimum [Prego et al., 2012]; it corresponds to a FDR length of $L_c = 15$ samples. At any frequency band, the value of L_c is iteratively decreased if no FDR is found, until a minimum value of 3 samples (96 ms). If still no FDR is found, the sound clip is discarded.

In order to compute α and β , we run the baseline method on both *development* datasets. For each IR, the mean and standard deviation of the results are computed across all sound clips. Then,

Table 3.1: Baseline system: linear regression parameters

Dataset	α	β	σ
Speech	6.6619	-1.4517	0.2131
Drums	8.2421	-2.1939	1.0055

these values are used for a *weighted least squares* linear regression against the true T_{60} values. The results are shown in Table 3.1, where σ represents the joint standard deviation of α and β after the linear regression; the resulting values are in the same range as the values reported in [Prego et al., 2012].

In the dereverberation stage, the STFT uses a small window size of 128 samples, with 64 samples overlap. The value of p is set to 0.25, given the good results reported in [Jukić et al., 2015]. Other parameter values are $\tau = 2$, $i_{max} = 10$, $\eta = 10^{-4}$ and $\epsilon = 10^{-4}$. After an exploratory search, the length of the IIR filter $L_g = 20$ has been chosen as a compromise between method performance and computation time. We have observed a tendency towards poor dereverberation and non-convergence of the IRSI when using small values of L_g and short audios.

For the SID, the recorded and dereverberated signals are reshaped into much larger STFTs, with a window size of 8 s and a hop size of 0.5 s. The predicted filter size is 1 s.

For both *evaluation* datasets, the two presented methods are employed; we will refer to them as *Baseline* and *MAR+SID*. Furthermore, with the aim of evaluating the performance of the SID method in an isolated manner, we have included a third method, *Oracle SID*. As its name suggests, it performs the System Identification step using the true anechoic signal.

Table 3.2: Experiment results

Metric	speech		drums	
	<i>Baseline</i>	<i>MAR+SID</i>	<i>Baseline</i>	<i>MAR+SID</i>
Bias	-0.0599	0.0305	0.1521	0.2568
MSE	0.6366	0.0594	13.9376	16.5261
ρ	0.8212	0.9848	0.3705	0.7552

3.5.3 Evaluation metrics

We have considered the three metrics from the ACE Challenge [Eaton et al., 2016], all of them based on the difference between estimated and true values: the *bias*, or mean error; the Mean Squared Error (*MSE*); and the Pearson correlation coefficient. The evaluation has been performed after discarding the outliers, defined as the reverberation time estimates greater than 1.5 s.

3.6 Results

Figure 3.1 shows the experiment result specified for all audio clips individually. Each boxplot represents the statistics of the mean estimation error (*bias*) for a single audio clip subject to all 9 different IRs. The results are organized by method (rows) and dataset (columns). Figure 3.2 aggregates all experiment results into the same plot, showing the statistical distribution of the *bias* per method and dataset. In this case, the *Oracle SID* results are omitted for clarity. The evaluation metrics for all methods are shown in Table 5.3.

According to the results, the proposed method clearly outperforms the baseline in the *speech* dataset by a tenfold MSE improvement. For the *drums* dataset, our method only outperforms the

baseline regarding correlation. Nevertheless, an inspection of the statistical distribution of mean estimation errors in Figure 3.2 brings in an interesting observation: the variability of the results given by our method is substantially smaller than the results of the baseline system. This behaviour is consistent across datasets: the mean error distributions with the *speech* dataset are approximately five times narrower than with the *drums* dataset, regardless of the method.

Moreover, all methods behave significantly better on the *speech* dataset. The main reason might be the heterogeneity of the *drums* dataset with respect to dynamic range or timbre, and the potential application of audio effects of any kind. Furthermore, some audio clips of the *drums* dataset contain sounds with a high degree of self-similarity, such as cymbal rolls or exaggerated reverbs; these characteristics would explain the outliers on the proposed method results. It is also interesting to notice the robustness of the proposed method against noise, present in the *speech* dataset. Such robustness is consistent with the behavior reported in [Jukić et al., 2015].

The performance of the *ORACLE SID* method is close to ideal. The *bias* is in all cases under 0.05 s (excepting a *drums* clip containing mostly silence). This result validates the system identification, and allows, in practical terms, a direct evaluation of the proposed method against the groundtruth values.

The results obtained in our analysis are very similar to the results reported in recent deep-learning state-of-the-art proposals, e.g. [Gamper and Tashev, 2018]. Since all those methods perform single-channel estimation, and our method requires FOA recordings, the results are not directly comparable. However, given the similar results obtained with the same evaluation metrics, it might be anticipated that our method may perform as well as other recent data-driven algorithms.

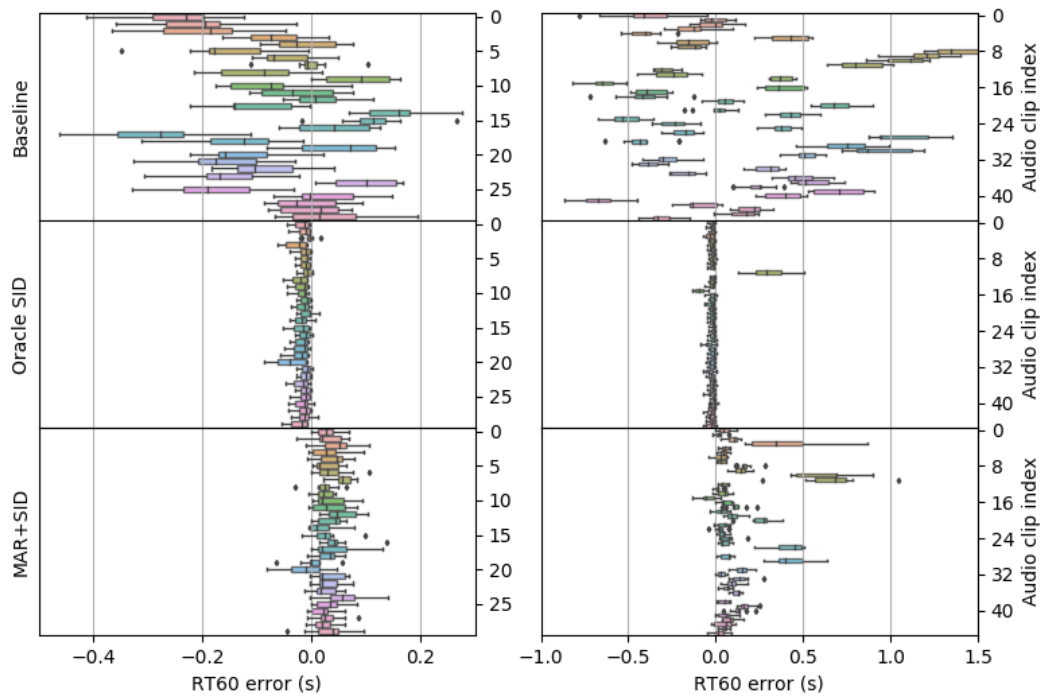


Figure 3.1: Experiment results for *speech* (left column) and *drums* (right column) datasets. Estimation error computed for each audio clip.

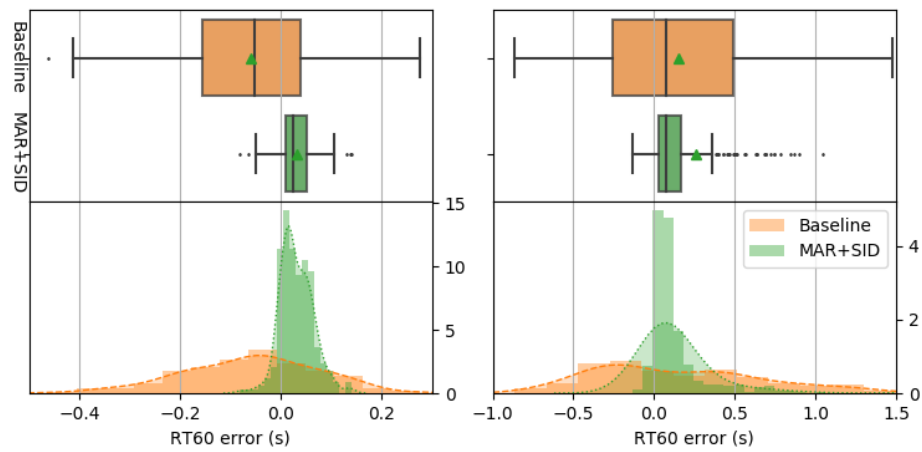


Figure 3.2: Experiment results for *speech* (left column) and *drums* (right column) datasets. Total estimation error across audio clips and acoustic conditions. Top: boxplot. Bottom: histogram and density plot

3.7 Conclusion

We have presented in this work a novel method for blind reverberation time estimation for multichannel audio, with the aim of applying it to the context of ambisonic recordings. Our method is based on a first dereverberation step, performed by a multichannel autoregressive model of the late reverberation. The resulting dry signal is then used to estimate the impulse response decay by means of system identification. The performance of the method is evaluated in a simulated experimental environment with two different reverberant datasets, and compared against a state-of-the-art method. Results show that our method outperforms the baseline method in a majority of evaluation metrics and conditions, and consistently provides results with less variability than the baseline method. In future work, we plan to extend the experimental setup by using recorded IRs. Furthermore, the proposed method could be extended to the case of moving sources by using an *online* autoregressive model. Finally, an extension of the method for higher ambisonic orders remains to be done.

Chapter 4

Coherence Estimation

4.1 Introduction

A number of practical applications benefit of the knowledge about the diffuseness of a sound field, including speech enhancement and dereverberation [P. Habets et al., 2006], noise suppression [Ito et al., 2010], source separation [Duong et al., 2009] or background estimation [Stefanakis and Mouchtaris, 2015]. In the field of spatial audio, diffuseness estimation is often used for parametrization [Pulkki, 2006, Politis et al., 2018], Direction-of-Arrival estimation [Thiergart et al., 2009] or source separation [Motlicek et al., 2013].

In this chapter, we study diffuseness estimation by subjecting a tetrahedral microphone array to spherically isotropic noise fields. The motivation for this work is, first, that tetrahedral arrays are a well known type of microphone arrays, which have today become popular for applications related to Virtual and Augmented Reality. Second, the spherical isotropic sound field is known to be a good approximation to the reverberant part of the sound field in a room [Elko, 2001, McCowan and Bourslard, 2003], and therefore it would be interesting to investigate how different microphone arrays behave under such conditions.

4.1.1 Problem definition

Under spherical isotropic noise, the theoretical coherence between any pair of zeroth- and first-order ambisonic virtual microphones is equal to 0 for all frequencies, due to the spherical harmonic orthogonality (Eq. 2.7) [Elko, 2001]. This result can also be assessed by Eq. (2.36).

However, there are several practical factors that might corrupt the coherence estimation, such as the approximation of the temporal expectation by time averaging [Thiergart et al., 2011] in Eq. (2.31), or the non-ideal implementation of the radial filters $\Gamma_n(kR)$ (Eq. 2.9) for the *A-B conversion* [Schörkhuber and Höldrich, 2017].

In the following sections, we present several experiments that illustrate the behavior of different coherence estimators applied on the signals captured with a tetrahedral microphone subjected to spherical isotropic noise, using both simulated and real sound recordings.

4.2 Methods

4.2.1 Simulation

Spherical isotropic noise has been generated following the *geometrical method* [Habets and Gannot, 2007, Habets and Gannot, 2010], using $I = 1024$ plane waves. The resulting *A-Format* signals correspond to a virtual tetrahedral microphone array mimicking the Ambeo¹ characteristics ($R = 0.015$ meter, $\alpha = 0.5$). The generated audio has a duration of 60 seconds.

¹Sennheiser Ambeo VR Mic. <https://en-us.sennheiser.com/microphone-3d-audio-ambeo-vr-mic>

4.2.2 Recording

Spherical isotropic noise has been rendered to a spherical loudspeaker layout with 25 *Genelec 8040*. The loudspeakers are arranged into three azimuth-equidistant 8-speaker rings at inclinations $\vartheta = [\pi/4, \pi/2, 3\pi/4]$, plus one speaker at the zenith. The different speaker distances to the center are delay- and gain-corrected, and the signal feeds are equalized to compensate for speaker coloration. The room has an approximate T_{60} of 300 ms measured at the 1 kHz third-band octave.

The spherical isotropic noise has been also created by the *geometrical method*, encoding a number of uncorrelated noise plane waves in ambisonics with varying orders $N \in [1, 5]$. Due to practical limitations related with the software, the minimum number of sources $I = 256$ for an accurate sound field reconstruction [Habets and Gannot, 2010] could not be reached - instead, the analysis has been performed parametrically with $I = [8, 16, 32, 64]$. For each value of N and I , approximately 15 seconds of audio have been recorded with an Ambeo microphone located at the center of the speaker array.

Ambisonics decoding is performed with an AllRAD decoder, passing through a spherical 64-point 10-design virtual speaker layout, and includes an imaginary speaker at the nadir. The decoding matrix uses *in-phase* weights.

4.2.3 Data processing and metrics

The sampling rate of all signals is 48 kHz. All frequency-domain results have been obtained by averaging their time-frequency representations over time. *A-B conversion* has been computed using *Ambeo A-B converter* AU plugin, version 1.2.1.

Two error metrics are considered: the frequency-dependent squared error $\varepsilon(k)$:

$$\varepsilon(k) = |X_1(k) - X_2(k)|^2, \quad (4.1)$$

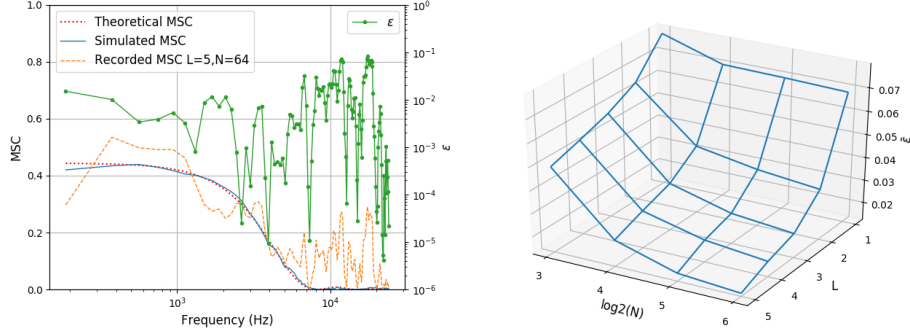


Figure 4.1: *A-Format* coherence between microphone signals. Left: MSC as a function of the frequency of theoretical, simulated and recorded ((BLD, BRU) , $N = 5$, $I = 64$) signals. Right: mean error $\bar{\varepsilon}$ of the recorded signals' MSC ((BLD, BRU)) compared to the simulated values, for all values of N and I . **REDO FIGURE WITH N AND I**

and the mean squared error $\bar{\varepsilon}$:

$$\bar{\varepsilon} = \frac{1}{K} \sum_{k=1}^K |X_1(k) - X_2(k)|^2 \quad (4.2)$$

4.3 Results and discussion

4.3.1 A-Format

The coherence of the generated *A-Format* signals is exemplified in Fig. 4.1 (left), which shows the *MSC* between the capsule pair (BLD, BRU) for the theoretical, simulated and recorded cases. The theoretical coherence is derived from Eq. (2.36), while simulated and recorded *MSC* have been computed by Welch's method, using a *hanning* window of 256 samples and 1/2 overlap. The difference between theoretical and simulated coherence is negligible for practical applications. However, there is a noticeable difference when

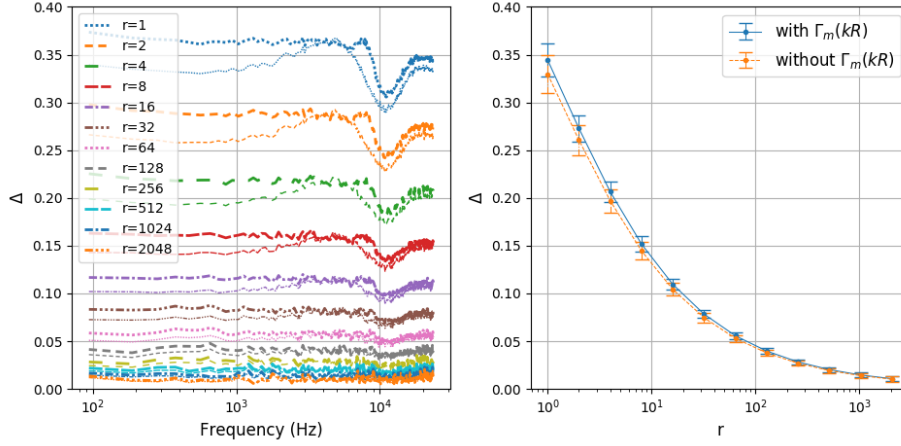


Figure 4.2: Estimated *B-Format* coherence (Δ) of a simulated diffuse sound field, as a function of the temporal averaging vicinity radius r . Left: $\Delta(k)$ for different values of r , with (coarse) and without (fine) application of radial filters. Right: mean and standard deviation of $\Delta(k)$ as a function of r .

compared to the recorded coherence. In general, the recorded MSC follows the tendency of the simulated curve up to around 5 kHz. Above this frequency, the recorded *MSC* presents several spectral peaks, which might be partially explained by the interference of the microphone itself in the recorded sound field, and by the non-ideal directivity of the capsules. The squared error $\varepsilon(k)$ with respect to the simulated curve is shown in Fig. 4.1 (left), while Fig. 4.1 (right) represents the same error averaged over frequency $\bar{\varepsilon}$ for different spatial resolution values of the diffuse field reproduction algorithm. As expected, $\bar{\varepsilon}$ decreases with increasing values of N and I .

4.3.2 B-Format

In order to evaluate the dependency of the *B-Format* coherence Δ on the number of time frames used for averaging, the following

procedure is presented. The simulated *A-Format* sound field has been transformed into the spherical harmonic domain, with and without the application of radial filters $\Gamma_n(kR)$ (Eq. 2.9). Then, Δ has been computed with Eq. (2.32) for exponentially growing values of r between 1 (8 ms) and 2048 (10.92 s), where r is the vicinity radius used for time averaging, and the number of time windows is given by $T = 2r + 1$. The time-frequency representation is derived by applying the STFT with the same window parameters as in Subsection 4.3.1.

Figure 4.2 (left) shows the great dependence of Δ on r . The estimated coherence tends to the theoretical values with increasing values of r . This tendency is better appreciated in Fig. 4.2 (right): the curve asymptotically decreases to a value $\Delta_{min} \approx 0$.

Another interesting observation comes from the frequency response of the curves. For all values of r , the coherence of the compensated *B-Format* signal (with $\Gamma_m(kR)$) is roughly flat up to around 7 kHz, which approximately corresponds to the operational spatial frequency range of the microphone [Gerzon, 1975a]. Above this value, the coherence response loses the flatness due to spatial aliasing (Eq. 2.11). The response above the maximum frequency could be stabilized, if needed, by alternative diffuseness estimation methods [Politis et al., 2015].

The coherence level differences along frequency are inversely proportional to r — the effect is better depicted by the standard deviation values (right). The effect of the radial filters in the coherence measurement is also shown: for a given r , the shape of the coherence is always less flat if no filters are applied. Conversely, in this case, coherence values are always smaller for the same r . This effect might be explained taking into account the inter-channel coherence introduced by microphone and encoder imperfections in real scenarios [Schörkhuber and Höldrich, 2017].

As a remark, the comparison between Figs. 4.1 and 4.2 provides evidence that the application of the spherical harmonic transform

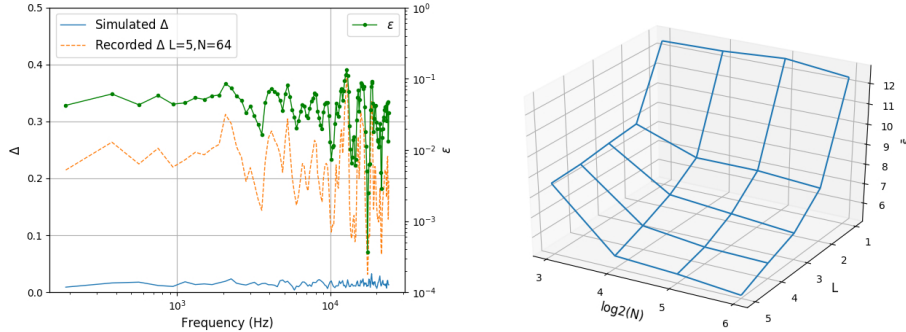


Figure 4.3: *B-Format coherence* between microphone signals. Left: Δ of simulated and recorded ($N = 5, I = 64$) signals. Right: $\bar{\varepsilon}$ of the recorded signals coherence across all values of N and I . **REDO FIGURE**

might be able to yield more accurate diffuseness estimations, due to a better signal conditioning [?].

Figure 4.3 (left) shows the estimated coherence for the recorded sound field with $N = 5$ and $I = 64$, using a vicinity radius of $r = 1024$ (≈ 5 s). The curve is centred around $\Delta = 0.25$ and presents several spectral peaks, as in the *A-Format* case. It is important to notice here that the deviations between the coherence of the simulated and the recorded sound fields are much stronger compared to those of Fig. 4.1.

This effect can be also appreciated in Fig. 4.3 (right): the mean squared error is around two orders of magnitude higher in *B-Format*. Nevertheless, similar as in Fig. 4.1 (right), $\bar{\varepsilon}$ decreases with increasing values of N and I . This behavior suggests that the deviations between the recorded and the simulated coherence can be to a large degree explained by the low spatial resolution of the reproduction system; given a higher number of loudspeakers, we expect that the reproduced diffuseness will tend to the theoretical expression.

4.4 Conclusions

The diffuseness of a sound field is an important parameter for several applications. In this work, two different metrics of diffuseness have been defined and measured with a tetrahedral microphone subjected to spherical isotropic noise.

The analysis shows, first, the impact of the time-averaging window length on the *B-Format* diffuseness estimator. This result might be useful for designing coherence estimators that are parametrized with respect to the length of the analysis window [[Thiergart et al., 2011](#)].

Second, the feasibility of diffuse sound field reproduction by a spherical loudspeaker array using ambisonics plane-wave encoding and the *geometrical method* is studied. Results suggest that this approach is viable, given a sufficient spatial resolution; a quantification of the impact of the number of loudspeakers remains for future work.

Chapter 5

Sound Event Localization and Detection

5.1 Introduction

Sound Event Localization and Detection (SELD) refers to the problem of identifying, for each individual event present in a sound field, the **spatial location** Ω , **temporal activity** Υ , and **sound class** κ to which it belongs.

The organization of a dedicated SELD task within the IEEE AASP Challenge on Detection and Classification of Acoustic Scenes and Events (DCASE) 2019 can be considered as a milestone for the development of the SELD research problem. Indeed, a large number of novel methodologies were developed for the Challenge, most of them based on Convolutional Recurrent Neural Networks (CRNN). The performance of the baseline method, a CRNN that performed jointly the localization and classification tasks [Adavanne et al., 2018], was vastly exceeded by a variety of deep-learning based algorithms [Kapka and Lewandowski, 2019, Cao et al., 2019, Grondin et al., 2019]. Some of these improvements have been included in the baseline system for the SELD Challenge of DCASE 2020.

Despite the predominant trend towards high-complexity deep-learning architectures, some recent works have been able to match or even improve CRNN-based methods with regard to localization, by using parametric analysis of the ambisonic sound field [Pérez-López et al., 2019, Nguyen et al., 2020]. Apart from the benefit derived by their simplicity, these approaches are able to resolve the case of overlapping events of the same class, a situation difficult to disambiguate for CRNN-based methods [Politis et al., 2020].

The present work continues the exploration of possibilities of parametric SELD methods, focusing on a low-complexity architecture that makes use of traditional, feature-based machine learning techniques. The method has been developed in the context of the SELD task within DCASE 2020 Challenge, and therefore utilizes the proposed dataset, baseline system and evaluation metrics.

Finally, it is important to remark that the method described here is the continuation of an algorithm presented at the DCASE 2019 Challenge [Pérez-López et al., 2019]; both algorithms share a common structure and a similar approach to the SELD problem. However, the current proposal tries to solve some of the problems identified on our early approach, mainly related with a low frame recall derived from a naive approach to event segmentation. Moreover, the current method also presents a complexity reduction, regarding the single-source DOA estimation and the classifier.

5.2 SYSTEM DESCRIPTION

The proposed method, referred to as *PAPAFIL*, can be summed up in four steps:

1. Estimate single-source time-frequency bins.
2. Use a particle tracking system to estimate event trajectories and activation times from single-source bins.
3. Perform spatio-temporal filtering on the input signal.

4. Assign a class label to the estimated event.

A scheme of the method is shown in Fig. 5.1.

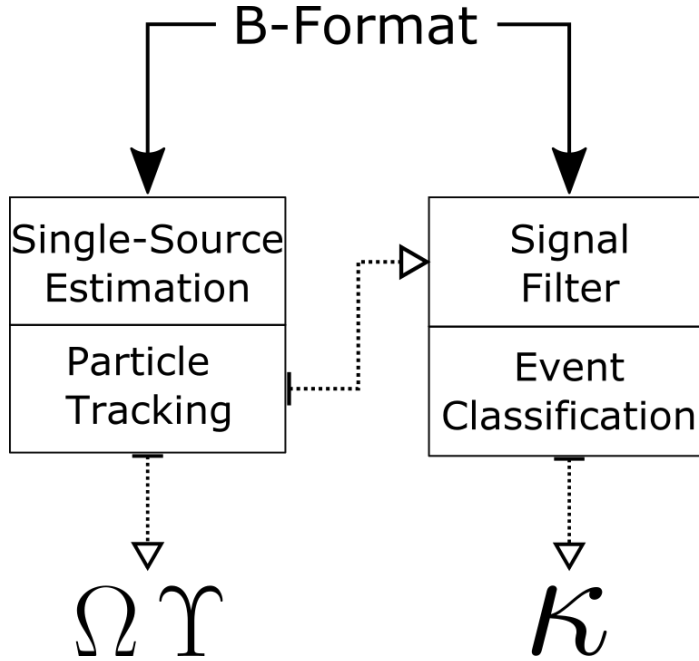


Figure 5.1: Architecture of the proposed methodology.

5.2.1 Single-source estimation

The first step is the transformation of the B-Format input signal $x_n^m(t)$ using the Short-Time Fourier Transform (STFT) into the time-frequency (TF) signal $X_n^m(k, n)$.

In the resulting spectrogram, the frequencies above a given limit f_{max} are discarded; this procedure speeds up the method while maintaining the directional information, given that the microphone geometry aliases spatial measurements above approx. 5 kHz [Bertet et al., 2006].

Assuming that the sources are sparse in time-frequency, it could be possible to identify TF bins which contain a significant energetic contribution from only one source. These bins could be then used to produce accurate DOA estimates. The effectiveness of this approach has already been demonstrated [Tho et al., 2014, Nguyen et al., 2020].

Single-source TF bins are computed from the DirAC parametric analysis. A variety of alternative subspace methods are known [Epain and Jin, 2016, Madmoni and Rafaely, 2018]; however, those methods require local estimation of eigenvalues, which is a computationally expensive procedure.

A TF bin is counted as single-source if its diffuseness $\Psi(k, n)$ is lower than a threshold Ψ_{max} . Diffuseness is computed here using Eq. 2.31. Finally, the DOA $\Omega(k, n)$ of the TF bins passing the aforementioned single-source test is computed as the angle of the active intensity vector by Eq. 2.29. To illustrate the process, an example of the method output is plotted in Fig. 5.2 (top).

5.2.2 Particle tracking

Once a set of reliable TF DOA estimates is obtained, the next step is the generalization of the individual measurements into trajectories and temporal activations. In our case, we opted for the Rao-Blackwellized Monte-Carlo Data Association (RBMCD) algorithm [Särkkä et al., 2004], which decomposes the multiple target tracking problem in two: it solves first the data association problem, and then performs the single target tracking individually. This method has been recently used in the context of sound event localization and tracking with successful results [Adavanne et al., 2018, Adavanne et al., 2019]; the code used for our implementation has been adapted from the same authors¹.

The system takes as the input the set of TF DOA values passing the single source test, and produces spatio-temporal event trajec-

¹<https://github.com/sharathadavanne/multiple-target-tracking>

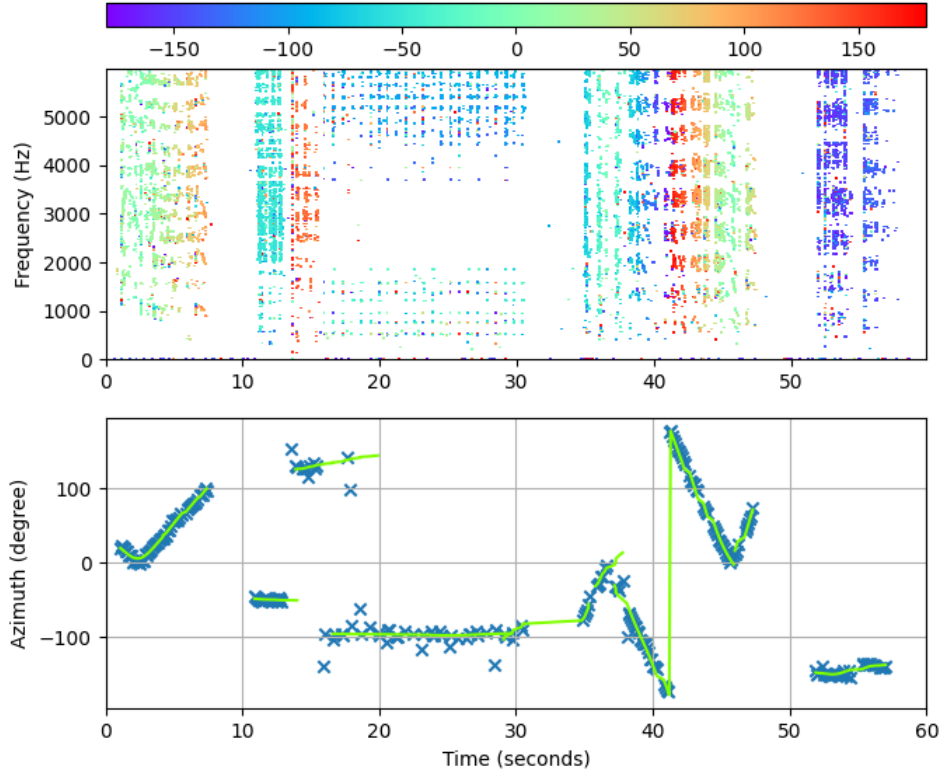


Figure 5.2: Estimation of localization and temporal activation. Top: azimuth spectrogram after diffuseness mask; color indicates estimated position of a TF bin passing the single-source test. Bottom: input/output of the particle tracking; the crosses represent the measurement space, and the continuous lines are the resulting events.

tories, considering an event as an entity with contiguous temporal activation and continuous spatial position. More specifically, for each time frame of the DOA masked spectrogram, the median² of all narrowband DOA estimates is computed. The resulting value is added to the measurement space of the tracker if the number of single-source frequency bins for that frame exceeds a minimum

²Circular median in the case of azimuth.

K_{min} .

The performance of the RBMCDA algorithm is controlled by several parameters. Some of the most relevant include the angular velocity prior v , the standard deviation σ_v and the spectral density s_v of the measurement noise, the prior probabilities of birth p_{birth} and noise percentage p_v , and the number of Monte-Carlo particles N . Position-related parameters are adjusted with respect to their ranges, so that azimuth-related magnitudes double elevation values.

The procedure is followed by a numerical post-processing step, which includes data interpolation, resampling (if needed), and removal of elements shorter than T_{min} . Finally, the system provides a list of J events, each one having an instantaneous position $\Omega_j(t)$ and a temporal activation Υ_j . An example of the system inputs and outputs is depicted in Fig. 5.2 (bottom).

5.2.3 Signal filter

The information provided by the particle tracking system is used to spatially filter the input signal. This can provide an enhanced monophonic estimate of an event $\tilde{s}_j(t)$ with reduced influence of simultaneous events. The process is performed by steering a virtual first-order cardioid in the direction of interest, using Eq. 2.15. The result of this process is a monophonic estimate for each event, $\tilde{s}_j(t)$, temporally delimited by Υ_j . As a last step, each estimate is amplitude peak-normalized, in order to minimize potential amplitude variability due to arbitrary configurations of the scene.

5.2.4 Event classification

As a final step, a class label is assigned to each estimated event $\tilde{s}_j(t)$ using a single-class classifier. Since the objective is to keep complexity low and make results interpretable, a machine learning algorithm is used instead of deep learning frameworks. The main

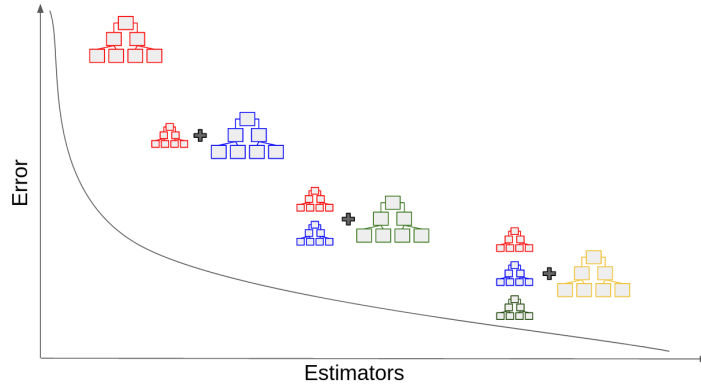


Figure 5.3: Gradient boosting machine learning process. Adding weak estimators allows reducing overall error in the predictions.

advantages of this choice are: (i) low number of parameters; (ii) low train and predict computational time, easing reproducibility; and (iii) relative importance of the features in the output can be interpreted, which is not possible with deep learning approaches.

Gradient Boosting Machine (GBM, Fig. 5.3) has been selected as the classification algorithm since it is a powerful yet simple technique for predictive modeling. In essence, the algorithm is aimed to minimize the loss of the objective function by adding many weak learners. These learners are typically simple decision trees and their parameters are tuned using gradient descent techniques. GBM implementation makes use of the *scikit-learn* library [Pedregosa et al., 2011].

Sound features are obtained using extractors from *Essentia*, an open-source library for audio analysis [Bogdanov et al., 2013]. Given the heterogeneous nature of the sound classes, a mixture of spectral, temporal and harmonic features are used, as shown in Table 5.1. Features are computed either frame-based or on the whole event; in the former case, the classifier is fed with their temporal first-order statistics.

Table 5.1: Acoustic features used for classification, grouped by type.

Type	Features	Number
<i>Low-level</i>	Mel bands	24
	MFCC	13
	Spectral Features	26
<i>SFX</i>	Duration	2
	Harmonic	4
	Sound envelope	11
	Pitch envelope	4

5.3 EXPERIMENTS

5.3.1 Dataset and baseline system

The dataset used is the FOA subset of the development set of the *TAU-NIGENS Spatial Sound Events 2020* [Politis et al., 2020], which features 600 different B-Format clips of 60 seconds long each. Each clip contains multiple sound events, which belong to one of the fourteen sound classes from the NIGENS database [Trowitzsch et al., 2019]. Events are also located at a potentially time-varying positions, and the maximum instantaneous overlapping of sources allowed is limited to two. Fifteen different Room Impulse Responses (RIR) are used for scene reverberation, covering a vast range of acoustic conditions. Furthermore, the audio clips contain a moderate amount of recorded background sounds.

The baseline method is based on the recently proposed SELDnet architecture [Adavanne et al., 2018], which features a Convolutional Recurrent Neural Network (CRNN) that solves both localization and classification problems jointly. Additionally, the baseline implementation has been improved with several changes inspired by one of the best performing methods in DCASE 2019 Task 3 Challenge [Cao et al., 2019].

5.3.2 Experimental setup

In order to explore the performance of the system, two different approaches have been undertaken regarding the creation of the training dataset for the monophonic single-class classifier. The first approach, referred to as *PAPAFIL1*, collects all event localization, temporal activation and class information by parsing the annotation files. Conversely, the second approach, called *PAPAFIL2*, uses the proposed parametric particle filter to estimate localizations and activations, and the class label is assigned to each event by a custom association algorithm based on spatio-temporal distance. In both cases, the input signal is filtered with the obtained information in order to conform the monophonic event estimates.

Therefore, the difference between training datasets is noticeable: while the training events in *PAPAFIL1* are more accurately determined than in *PAPAFIL2*, the differences with respect to the prediction scenario are much bigger in the former case. The number of individual events for each of the approaches is plotted in Fig. 5.4. Approximately half of the classes have similar number of instances in both datasets. However, the other half presents noticeable differences, which might be explained by the different criteria applied for the consideration of event temporal activations: the groundtruth seems to follow a frame-based activity detection approach, while the output of the proposed method tends to consider events as time-continuous manifestations, influenced by the particle filter.

This situation leads to two different *oracle* systems (referred to by appending -*O* in the method name), which represent the best performance theoretically achievable for the corresponding method.

The accurate information of the *PAPAFIL1* training set suggests a need for data augmentation; in contrast, the training material used in *PAPAFIL2* is already provided by a certain extent of variability. This situation motivates the implementation of data augmentation methods in the *PAPAFIL1* training set. Specifically, several standard

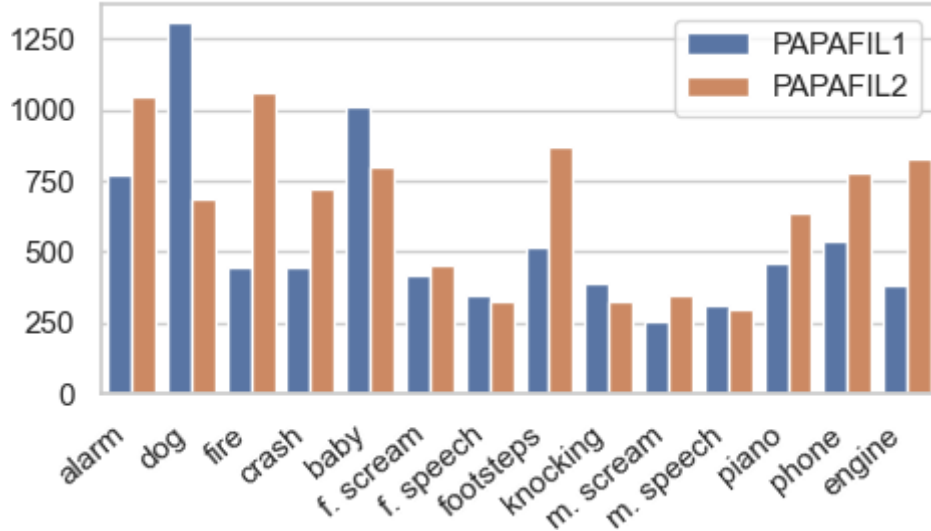


Figure 5.4: Number of occurrences of each event class in the training set, for both proposed methods.

data augmentation techniques are implemented: pitch shifting, time shifting, time stretching and white noise addition. Furthermore, given the observed high influence of reverberation in the system performance, a reverberant data augmentation technique based on synthetic RIRs has been considered. Ten different single-channel RIRs, with reverberation times between 0.3 and 1.1 seconds, have been synthetically created using the *masp* library [Pérez-López and Politis, 2020]. During training, each event estimate is convolved with one of the RIRs, randomly chosen. RIR augmentation has recently been shown very effective for blind reverberation time estimation [Bryan, 2020] but, to the best of the authors’ knowledge, this is the first application in SELD.

Table 5.2 shows a comprehensive list of the parameters used throughout the different steps of the proposed method. All values are equal for both presented approaches, except for the number of Monte-Carlo particles N . The values for Single-Source Estima-

tion and Particle Filtering parameters have been iteratively refined by manual tuning and inspection, departing from standard values. The beamforming weights α_m correspond to the *maximum directivity beamformer*, which minimizes the energy contributions from directions other than the lookup direction [Rafaely, 2015]. In the spatial audio field, such property is also known as the *max-rE* decoder [Daniel, 2000]. Regarding event classification, a cross-validation scheme has been implemented for tuning GBM hyperparameters.

5.3.3 Evaluation metrics

The system is evaluated according to the joint metrics proposed in the Challenge [Mesaros et al., 2019]. The metrics evaluate jointly the localization and the classification, and are divided into two types: location-aware classification, and classification-aware localization. There are two classification metrics: Error Rate (ER_{20}) and F-Score (F_{20}). As the name suggests, the metrics are conditioned to a minimum localization performance, which is set to 20° in this case. Localization metrics are also two-fold: Localization Error (LE_{CD}) and Localization Recall (LR_{CD}); as their name suggests, the metrics are class-dependent, and thus are conditioned to a correct classification. Finally, the SELD score is an average of the four other metrics, used to conveniently sum up the results.

5.4 RESULTS

Table 5.3 summarizes the results of the experiments using the recommended data split: training with folds 3 to 6, validation with fold 2 and testing with fold 1. Results are reported for three different systems: the baseline and the two proposed methods *PAPAFIL1* and *PAPAFIL2*. The results of their respective oracle results, *PAPAFIL1-O* and *PAPAFIL2-O*, are also provided.

Table 5.2: (Hyper-)parameter values.

Step	Parameter	Value	Unit
Single-Source	sample rate	24	kHz
	window size	2400	samples
	window overlap	50	%
	f_{max}	6	kHz
	N_{Ψ}	2	frames
	Ψ_{max}	0.1	
Particle Filtering	v	2	°/frame
	σ_{ν}	5	
	s_{ν}	20	
	p_{birth}	0.25	
	p_{ν}	0.25	
	N	100 / 30	
	K_{min}	10	bins/frame
	T_{min}	10	frames
Signal	α_0	0.775	
Filter	α_1	3 * 0.4	
Event Classification	number of estimators	1300	trees
	loss	$mlogloss$	
	learning rate	0.05	
	max depth	4	
	min samples leaf	10	samples

Both proposed approaches outperform the baseline system in three out of the four evaluation metrics (ER_{20} , F_{20} and LE_{CD}). Although the results obtained by both of them are similar, *PAPAFIL2* obtains better classification scores (ER_{20} and F_{20}), and *PAPAFIL1* performs subtly better regarding localization error (LE_{CD}). However, the localization recall results (LR_{CD}) are slightly worst than the baseline in both cases. This fact does not prevent the proposed methods to have a SELD score better than the baseline: 0.41 (*PA-*

PAPAFIL1) and 0.38 (*PAPAFIL2*), against 0.47 (*BASELINE*).

The results obtained by the oracle methods are within the expected ranges. *PAPAFIL1-O* performs almost perfectly regarding LE_{CD} , but the classification errors influence the LR_{CD} result. In turn, *PAPAFIL2-O* performs better than *PAPAFIL1-O* regarding all metrics, excepting LE_{CD} ; this improvement is specially noticeable in LR_{CD} , with a performance difference of about 15%. The good results obtained by *PAPAFIL2-O* validate the proposed particle filtering approach, an leave space for improvements that might be given by a better understanding and fine tuning of the model.

The performance of the proposed methods deteriorates noticeably with overlapping sounds. A closer inspection reveals that, in many occasions, the TF bins passing the single-source test mostly belong to one out of two simultaneous sources. It is a known issue that performance of DirAC diffuseness is reduced when two sources are present [Epain and Jin, 2016]; similar problems have been reported in [Adavanne et al., 2019], where an instantaneous source number estimator is used in combination with the particle filter. As in that case, the results suggest the need for more sophisticated source detection and counting methods.

Table 5.3: Evaluation results on the development set.

Method	ER ₂₀	F ₂₀	LE _{CD}	LR _{CD}	SELD
<i>BASELINE</i>	0.72	37.4 %	22.8°	60.7 %	0.47
<i>PAPAFIL1</i>	0.60	49.8 %	13.4°	54.4 %	0.41
<i>PAPAFIL2</i>	0.57	54.0 %	13.8°	59.7 %	0.38
<i>PAPAFIL1-O</i>	0.37	67.0 %	2.0°	68.6 %	0.26
<i>PAPAFIL2-O</i>	0.32	79.6 %	8.5°	82.4%	0.19

To conclude the analysis, Fig. 5.5 shows the relative importance of the fifteen most relevant acoustic features for the *PAPAFIL2* classifier model. Event duration is clearly the feature with the highest

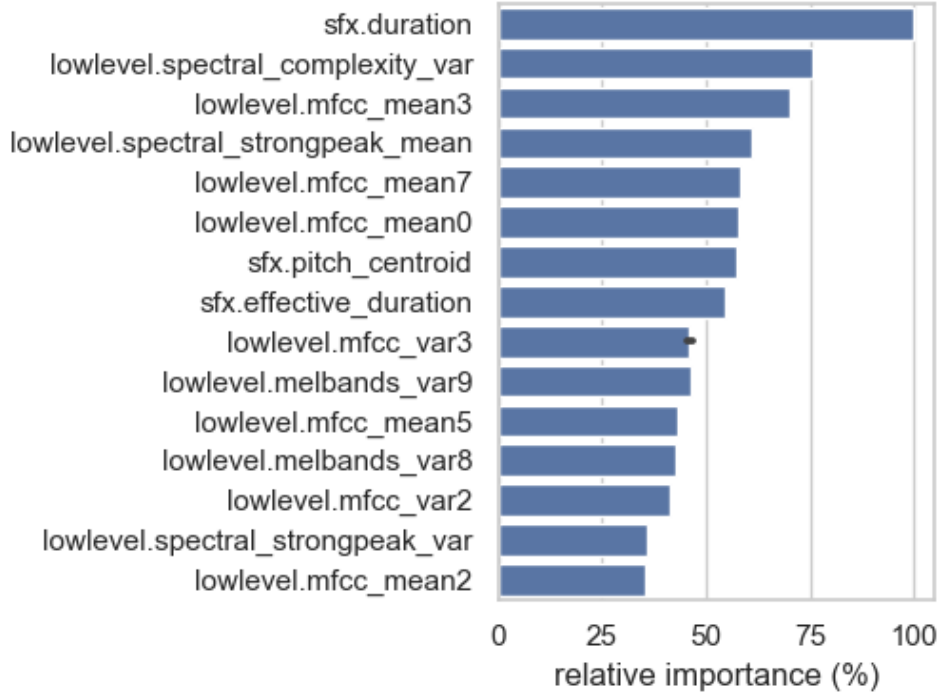


Figure 5.5: Most representative features in event classifier.

importance, and effective duration (duration of the signal discarding silence) also appears in the eighth position. This fact can help to explain the better performance of *PAPAFIL2* over *PAPAFIL1*: the temporal activities of the events in training and prediction are much more similar to each other in the former method, as a consequence of the training set generation approach. Furthermore, it is interesting to notice the high relevance of low-level features, and specifically several MFCC combinations (eight of the fifteen reported features) and various extractors related to the spectral structure. The absence of pitch, harmonic and envelope features in the list represents a significant finding as well.

TODO: DISCUSS RESULTS OF EVALUATION SET!!

5.5 Conclusion

We present a novel low-complexity method for Sound Event Localization and Detection of First Order Ambisonic signals, based on four steps: estimation of single-source spectrogram regions by parametric analysis; computation of event trajectories and activations by means of a particle tracker; spatio-temporal filtering of the input signal; and single-class monophonic event classification by Gradient Boosting. Results show that the proposed method outperforms the baseline method, a state-of-the-art Convolutional Recurrent Neural Network. Specifically, our method is able to improve the baseline SELD score by almost ten points, while increasing the scores in three out of the four metrics under consideration.

Chapter 6

Data generation and storage

6.1 Introduction

This chapter gathers several proposals related with the creation, storage and transmission of ambisonic data for research purposes. The main objective of the contributions described here is the support for the generation of parametrizable ambisonic datasets, using both synthetic and recorded materials, and specifically emphasizing the usage of Room Impulse Responses.

Most of the contributions listed here (and also most of the code developed for this thesis) have been implemented in Python. Indeed, Python has recently become one of the most used programming languages worldwide [[Robinson, 2017](#), [PYPL, 2020](#), [TIOBE, 2020](#)]; as shown also in Figure 6.1.

One of the reasons behind this tendency shift is the popularity of the language among machine learning and data science communities, fields where Python holds the first place by usage [[Elliott, 2019](#)]. Since data-driven paradigms currently conform the state-of-the-art of many applied sciences, including audio signal processing, the availability of convenience Python packages and libraries

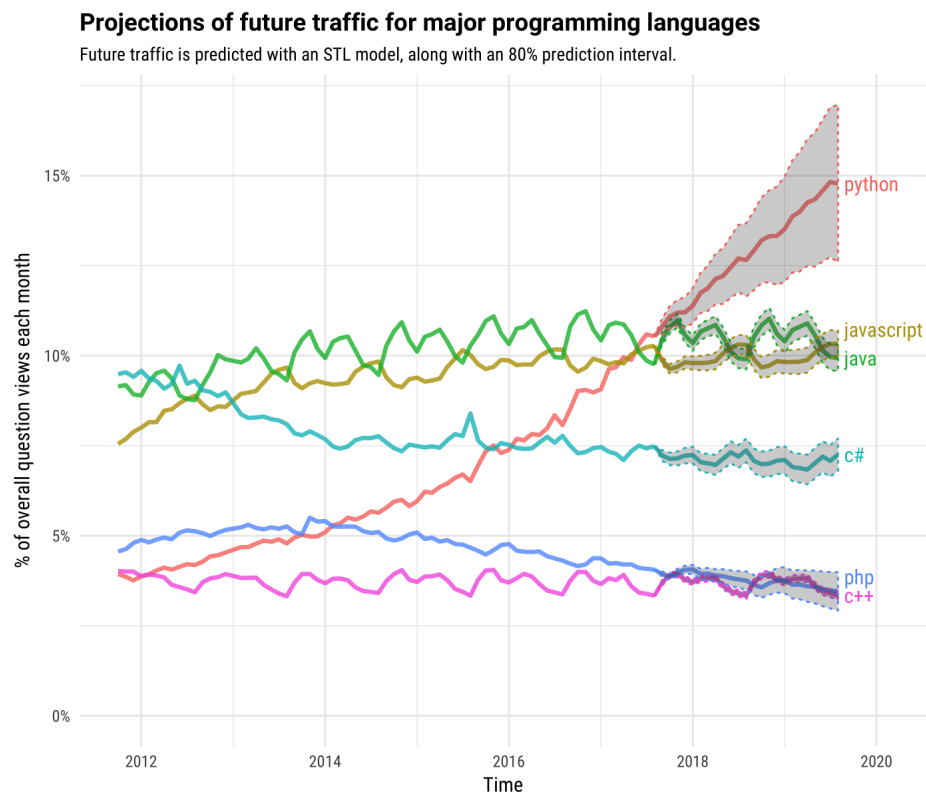


Figure 6.1: 2018 projections of future internet traffic for major programming languages. Adapted from [Robinson, 2017].

is therefore of the highest interest to the research community.

It is important to remark the predominant position that Matlab has always had regarding scientific computing. Indeed, it is still the tool of choice for many researchers, and the availability of libraries is accordingly very high. But the aforementioned tendency shift towards Python causes, as a side effect, the lack of many tools developed in Matlab by the research community.

Although Matlab code can be called and executed from Python, in practice this approach is suboptimal under several criteria. A better solution in the long run is the effective port of the code towards native Python code. Some of the libraries presented in this Chapter are partially or totally motivated by this scenario.

6.2 MASP: a Python library for multichannel acoustic signal processing

6.2.1 Description

The Multichannel Acoustic Signal Processing (*MASP*) is a Python library consisting of a collection of methods related with acoustics and microphone array processing. The library is mostly a transcoding from several Matlab libraries by A. Politis [Politis, 2016, Politis, 2020]. It can be conveniently installed using *pip*.

MASP implements a variety of methods for the simulation and analysis of reverberant acoustic scenes, with emphasis on microphone arrays with spherical geometries. More specifically, *MASP* is structured in submodules, with the following structure :

Array Response Simulator Simulation of spherical microphones:

- Rigid/open configurations.
- Scattering simulation.
- Arbitrary capsule distances, positions and directivities.

Shoebox Room Model Fast implementation of the Image Source Method [[Allen and Berkley, 1979](#)]:

- Convex 3D rooms.
- Arbitrary number of sources and receivers, with arbitrary positions, orientations and directivities.
- ISM expansion limited by order or time.
- Frequency-dependent wall absorption.
- RIR with spherical harmonic expansion.

Spherical Array Processing Transformation and analysis of signals measured with a spherical microphone array:

- A2B conversion with theoretical or measured filters.
- Signal-independent beamforming.
- Signal-dependent and adaptive beamforming.
- Direction of Arrival estimation.
- Diffuseness estimation.

Spherical Harmonic Transform Mathematical convenience tools.

The library implements a Unit Testing system, which numerically assesses the validity of the methods. More specifically, each function test calls the equivalent Matlab code under the hood. The numeric result is then sent back to Python, where it is evaluated against the own result.

Two example applications of the library are shown in [Figures 6.2 and 6.3](#). In [Figure 6.2](#), obtained with the Array Response Simulator package, the frequency response of a spherical microphone array to an impinging plane-wave with varying incidence angle is shown. The microphone array consists of a 2nd order supercardioid and a 3rd order hypercardioid, located at opposite directions of an open

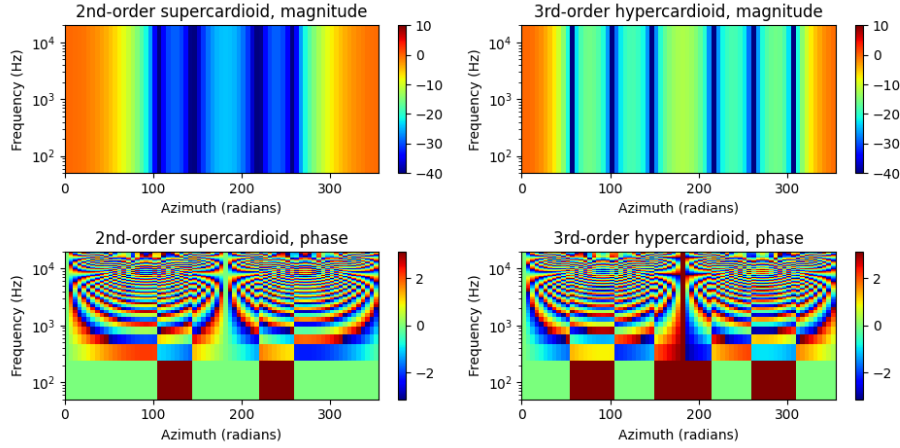


Figure 6.2: Frequency response of an arbitrary spherical array.

sphere, and both of them facing to the front direction.

One of the features of the Spherical Array Processing package is shown in Figure 6.3. The plot shows the evaluation of radial filters $\Gamma_n(kR)$ for an arbitrary spherical array, generated by inverting the theoretical response of the array [Bertet et al., 2006]. The evaluation is performed following the metrics presented in the same paper, which compare spatial correlation, level difference and maximum amplification with respect to the ideal case.

6.2.2 Related software

There exists another recent Python library which covers a similar scope: *pyroomacoustics* [Scheibler et al., 2018]. This framework provides an object-oriented interface with two main application scopes: allow RIR simulation of complex rooms based on the image source method, and provide a reference implementation of standard microphone array processing algorithms.

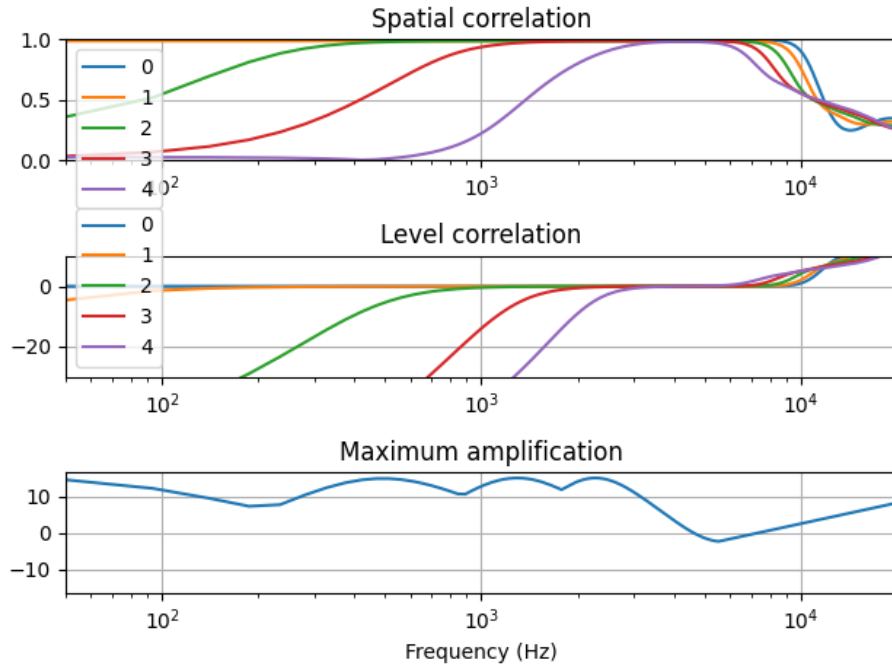


Figure 6.3: Evaluation of radial filters for an arbitrary spherical microphone array.

Although some of the features are common to both libraries, there is a significant difference regarding their target usage. While *MASP* primarily focuses on spherical geometries, *pyroomacoustics* is more concerned about arbitrary room geometries and computational performance. Therefore, both libraries might be considered as complementary to some extent. A comparative list of their features is shown in Table 6.1.

Table 6.1: Features of *MASP* compared to *pyroomacoustics*.

Package	Feature	MASP	PRA
Shoebox Room Model	Convex 3D room	✓	✓
	Non-convex 3D room	-	✓
	Arbitrary #sources	✓	✓
	Arbitrary #receivers, arrays	✓	✓
	ISM by max_order	✓	✓
	ISM by max_time	✓	-
	Wall absorption	✓	✓
	Frequency-dependent absorption	✓	-
	Plot methods	-	✓
	RIR rendering	✓	✓
	Audio simulation	✓	✓
	Acoustic descriptor estimation	✓	-
	Microphone orientation	✓	-
	Custom microphone directivity	✓	-
	RIR Spherical Harmonic Expansion	✓	-
Array Simulator	Rigid spherical arrays	✓	-
	Arbitrary capsule geometries	✓	-
	Recorded array IRs	✓	-
Spherical Processing	A2B conversion	✓	-
	Beamforming	✓	✓
	Plane-wave decomposition	✓	-
	Nullformer	✓	-
	Adaptive Beamforming	✓	-
	Adaptive Filtering	-	✓
	DoA Estimation	✓	✓
	Diffuseness Estimation	✓	-
	Diffuse-field coherence	✓	-
	Blind Source Separation	-	✓

6.3 SOFA

6.3.1 Problem statement

The availability of recorded room impulse responses is of great importance to many acoustic signal processing problems. Many different RIRs can be obtained from the same room, just by varying the position of the source and the receiver; when the number of source and receiver positions increases, the total amount of measurements increases geometrically. Besides that, the final format and organisation of the produced data (not only the RIR themselves, but also the source/position annotations) can be arbitrarily different when produced by different groups of people.

In order to overcome potential interoperability and reusability issues, the *Spatially Oriented Format for Acoustics* (SOFA) convention [Majdak et al., 2013], also known as the AES-69 standard [Majdak and Noisternig, 2015], proposes a unified file format for the storage of IR-related data. Despite that SOFA was initially created with an emphasis on *Head-Related Impulse Response* (HRIR) data, the framework that SOFA provides can be potentially applied to a variety of recording procedures and audio-related data. Such variety is associated with the concept of *conventions*: a specific data structure designed to hold a concrete type of data or measurement. Some examples of widespread conventions might be *SimpleFreeFieldHRIR* (for anechoic binaural measurements), *Simple-HeadphoneIR* (intended for storing headphone impulse responses), or *MultiSpeakerBRIR* (for binaural RIRs measured from loudspeaker arrays), to name a few of them.

6.3.2 Ambisonics Directional Room Impulse Response as a SOFA convention

Given the intrinsic spatial characterization capabilities of ambisonics, Gerzon proposed the technique as a potentially successful

candidate format for acoustical heritage preservation, as early as 1975 [Gerzon, 1975b].

The increase in popularity of ambisonics since the beginning of the present century has turned this idea into reality; OpenAIRlib, a freely accessible dataset that gathers dozens of RIRs, might be a good example of it [OpenAIRlib, 2020].

In any case, the usage of recorded ambisonic RIRs is not limited to the field of acoustic heritage. Among others, the availability of such recordings has powered works in a variety of works, auralization [Postma et al., 2016], room acoustics analysis [Embrechts, 2015, Clapp et al., 2011] and modelling [Romblom, 2017], spatial audio synthesis [Coleman et al., 2017] or source separation [Baqué et al., 2016].

In general, all publicly available ambisonic RIR measurements share some common approaches for describing and organizing the recorded data. For instance, recordings from different rooms are usually stored as separated folders. Each combination of emitter and receiver positions is often saved as an individual file, and the different spherical harmonics match the audio channels. Moreover, it is also usual to provide a *metadata* file, describing the different emitter and receiver positions, and potentially some information about the measurement setup, methodology, etc. Such files might be formatted as plain text or delimiter-separated files.

Despite the common approach, it can be easily foreseen that each database generated by a different individual or institution might potentially have a different naming convention, folder structure, file format, and so on. This is exactly the same situation that motivated the development of the SOFA conventions.

On the other hand, the SOFA specification defines some criteria that must be fulfilled in order to propose a new convention [SOFA, 2018]. These criteria are:

1. Data must exist.

2. Data can not be described by existing SOFA conventions.
3. Relevant information about the data must be available.

Given that the described situation meets all requirements, the *Ambisonics Directional Room Impulse Response* (AmbisonicsDRIR) convention has been therefore proposed as a new member of SOFA.

The technical specifications of the proposed convention in its current state (version 0.2) are available online [[Pérez-López and de Muynke, 2018](#)]. Despite a timid adoption of the convention, the AmbisonicsDRIR proposal has arisen interest in the community. At the moment of writing, the *Standardisation Committee on AES-69 Standard* is discussing potential modifications to the SOFA file format required for the adoption of several new features; and the support for spherical harmonic-based measurements is among the topics for deliberation.

6.3.3 pysofaconventions

The situation described in Section , regarding the availability of acoustic signal processing libraries in the Python programming language, can be easily extended to the case of SOFA APIs.

The library *pysofaconventions* has been created with the aim to provide an alternative to the existing Matlab/Octave and C/C++ implementations. For ease of installation, it is integrated in the standard python package manager, *pip*.

The current software version is 0.1.5. The library structure is inspired by the C++ implementation [[Carpentier, 2018](#)]. It features all functionalities described by SOFA version 1.0, plus the proposed AmbisonicsDRIR convention. The implementation is based on extensive error checking, to ensure code consistency.

pysofaconventions has gained a moderate amount of attraction. Among others, it is being used as a dependency for the *Real-Time Spherical Microphone Renderer (ReTiSAR) for binaural reproduction*,

developed by Chalmers University in collaboration with Facebook Reality Labs [[Helmholz et al., 2019](#)].

6.4 Ambiscaper

Chapter 7

Conclusions

7.1 Summary of Contributions

is that needed here?

- Academic Contributions
 1. Blind reverberation time estimation from ambisonic recordings **ref**
 - **Parameter estimation:** Novel technique for blind RT60 estimation of ambisonic recordings from autoregressive models
 2. Analysis of spherical isotropic noise fields with an A-Format tetrahedral microphone **ref**
 - **Parameter estimation:** Contribution to the characterization of coherence with tetrahedral microphones (the most common spherical arrangement)
 3. A hybrid parametric-deep learning approach for sound event localization and detection **ref**
 - **Scene Description:** Novel state-of-the-Art methodology for Sound Event Localization and Detection

- Software Contributions
 1. Ambiscaper: A Tool for Automatic Generation and Annotation of Reverberant Ambisonics Sound Scenes [ref](#)
 - **Data Generation:** Novel tool for reverberant ambisonic dataset generation
 2. Ambisonics Directional Room Impulse Response as a New Convention of the Spatially Oriented Format for Acoustics [ref](#)
 - **Recorded IRs:** File standard/convention proposal for storage of recorded ambisonic IRs
 3. A Python library for Multichannel Acoustic Signal Processing [ref](#)
 - **Simulated IRs:** Library for acoustic simulation (IR generation, microphone array simulation, etc)
 4. pysofaconventions, a Python API for SOFA [ref](#)
 - **Recorded IRs:** implementation of SOFA for python

7.2 Conclusion

7.3 Future work

Bibliography

- [Adavanne et al., 2018] Adavanne, S., Politis, A., Nikunen, J., and Virtanen, T. (2018). Sound event localization and detection of overlapping sources using convolutional recurrent neural networks. *IEEE Journal of Selected Topics in Signal Processing*, 13(1):34–48.
- [Adavanne et al., 2019] Adavanne, S., Politis, A., and Virtanen, T. (2019). Localization, detection and tracking of multiple moving sound sources with a convolutional recurrent neural network. *arXiv preprint arXiv:1904.12769*.
- [Ahonen and Pulkki, 2009] Ahonen, J. and Pulkki, V. (2009). Diffuseness estimation using temporal variation of intensity vectors. In *2009 IEEE Workshop on Applications of Signal Processing to Audio and Acoustics*, pages 285–288. IEEE.
- [Allen and Berkley, 1979] Allen, J. and Berkley, D. (1979). Image method for efficiently simulating small-room acoustics. *The Journal of the Acoustical Society of America*, 65(4):943–950.
- [Avargel and Cohen, 2007] Avargel, Y. and Cohen, I. (2007). On multiplicative transfer function approximation in the short-time fourier transform domain. *IEEE Signal Processing Letters*, 14(5):337–340.
- [Baqué et al., 2016] Baqué, M., Guérin, A., and Melon, M. (2016). Separation of direct sounds from early reflections using the en-

- trophy rate bound minimization algorithm. In *Audio Engineering Society Conference: 60th International Conference: DREAMS (Dereverberation and Reverberation of Audio, Music, and Speech)*. Audio Engineering Society.
- [BBCNews, 2016] BBCNews (2016). Mwc 2016: Zuckerberg takes samsung into a vr future. <https://www.bbc.com/news/technology-35629322>. Accessed on June 11th, 2020.
- [Begault and Trejo, 2000] Begault, D. R. and Trejo, L. J. (2000). 3-d sound for virtual reality and multimedia.
- [Bertet et al., 2006] Bertet, S., Daniel, J., and Moreau, S. (2006). 3D Sound Field Recording With Higher Order Ambisonics - Objective Measurements and Validation of a 4th Order Spherical Microphone. In *Proc. 120th AES Convention*, pages 1–24, Paris, France.
- [Bogdanov et al., 2013] Bogdanov, D., Wack, N., Gómez Gutiérrez, E., Gulati, S., Boyer, H., Mayor, O., Roma Trepas, G., Salamon, J., Zapata González, J. R., Serra, X., et al. (2013). Essentia: An audio analysis library for music information retrieval. In *14th Conference of the International Society for Music Information Retrieval (ISMIR)*; p. 493-8., Curitiba, Brazil.
- [Braun, 2018] Braun, S. (2018). *Speech dereverberation in noisy environments using time-frequency domain signal models*. PhD thesis, Friedrich-Alexander-Universität Erlangen-Nürnberg.
- [Braun and Habets, 2016] Braun, S. and Habets, E. A. (2016). On-line dereverberation for dynamic scenarios using a kalman filter with an autoregressive model. *IEEE Signal Processing Letters*, 23(12):1741–1745.
- [Braun et al., 2018] Braun, S., Kuklasinski, A., Schwartz, O., Thiergart, O., Habets, E. A., Gannot, S., Doclo, S., and Jensen, J. (2018).

- Evaluation and comparison of late reverberation power spectral density estimators. *IEEE/ACM Transactions on Audio, Speech, and Language Processing*, 26(6):1056–1071.
- [Bryan, 2020] Bryan, N. J. (2020). Impulse response data augmentation and deep neural networks for blind room acoustic parameter estimation. In *Proc. IEEE ICASSP*, Barcelona, Spain. IEEE.
- [Cao et al., 2019] Cao, Y., Kong, Q., Iqbal, T., An, F., Wang, W., and Plumbley, M. (2019). Polyphonic sound event detection and localization using a two-stage strategy. In *Proceedings of the Detection and Classification of Acoustic Scenes and Events 2019 Workshop (DCASE2019)*, pages 30–34, New York University, NY, USA.
- [Carpentier, 2017] Carpentier, T. (2017). Ambisonic spatial blur. In *142nd Audio Engineering Society Convention*. AES.
- [Carpentier, 2018] Carpentier, T. (2018). `Api_cpp`. https://github.com/sofacoustics/API_Cpp. Accessed on June 26th, 2020.
- [Chartrand and Yin, 2008] Chartrand, R. and Yin, W. (2008). Iteratively reweighted algorithms for compressive sensing. In *2008 IEEE International Conference on Acoustics, Speech and Signal Processing*, pages 3869–3872. IEEE.
- [Clapp et al., 2011] Clapp, S. W., Guthrie, A. E., Braasch, J., and Xiang, N. (2011). Investigations of room acoustics with a spherical microphone array. In *Audio Engineering Society Convention 131*. Audio Engineering Society.
- [Coleman et al., 2017] Coleman, P., Franck, A., Menzies, D., and Jackson, P. J. (2017). Object-based reverberation encoding from first-order ambisonic rirs. In *Audio Engineering Society Convention 142*. Audio Engineering Society.

- [Daniel, 2000] Daniel, J. (2000). *Représentation de champs acoustiques, application à la transmission et à la reproduction de scènes sonores complexes dans un contexte multimédia*. PhD thesis, University of Paris VI.
- [Drossos et al., 2017] Drossos, K., Adavanne, S., and Virtanen, T. (2017). Automated audio captioning with recurrent neural networks. In *2017 IEEE Workshop on Applications of Signal Processing to Audio and Acoustics (WASPAA)*, pages 374–378. IEEE.
- [Duong et al., 2009] Duong, N., Vincent, E., and Gribonval, R. (2009). Under-determined reverberant audio source separation using a full-rank spatial covariance model. *arXiv:0912.0171 [stat]*. arXiv: 0912.0171.
- [Eaton et al., 2016] Eaton, J., Gaubitch, N. D., Moore, A. H., and Naylor, P. A. (2016). Estimation of room acoustic parameters: The ace challenge. *IEEE/ACM Transactions on Audio, Speech, and Language Processing*, 24(10):1681–1693.
- [Elko, 2001] Elko, G. W. (2001). Spatial coherence functions for differential microphones in isotropic noise fields. In *Microphone Arrays*, pages 61–85. Springer, New York.
- [Elliott, 2019] Elliott, T. (2019). The state of the octoverse: machine learning. <https://github.blog/2019-01-24-the-state-of-the-octoverse-machine-learning/>. Accessed on June 26th, 2020.
- [Embrechts, 2015] Embrechts, J.-J. (2015). Measurement of 3d room impulse responses with a spherical microphone array. In *Proceedings of the Euronoise 2015 Congress*, pages 143–148.
- [Epain and Jin, 2016] Epain, N. and Jin, C. T. (2016). Spherical harmonic signal covariance and sound field diffuseness. *IEEE/ACM Transactions on Audio, Speech, and Language Processing*, 24(10):1796–1807.

- [Facebook, 2014] Facebook (2014). Facebook to acquire oculus. <https://about.fb.com/news/2014/03/facebook-to-acquire-oculus/>. Accessed on June 11th, 2020.
- [Fahy and Salmon, 1990] Fahy, F. J. and Salmon, V. (1990). *Sound intensity*. Acoustical Society of America.
- [Fortune, 2019] Fortune (2019). The fall and rise of vr: The struggle to make virtual reality get real. <https://fortune.com/longform/virtual-reality-struggle-hope-vr/>. Accessed on June 11th, 2020.
- [Gamper and Tashev, 2018] Gamper, H. and Tashev, I. J. (2018). Blind reverberation time estimation using a convolutional neural network. In *2018 16th International Workshop on Acoustic Signal Enhancement (IWAENC)*, pages 136–140. IEEE.
- [Gannot et al., 2017] Gannot, S., Vincent, E., Markovich-Golan, S., and Ozerov, A. (2017). A consolidated perspective on multimicrophone speech enhancement and source separation. *IEEE/ACM Transactions on Audio, Speech, and Language Processing*, 25(4):692–730.
- [Gerzon, 1973] Gerzon, M. (1973). Periphony: With-height sound reproduction. *Journal of the Audio Engineering Society*, 21(1):2–10.
- [Gerzon, 1975a] Gerzon, M. A. (1975a). The design of precisely coincident microphone arrays for stereo and surround sound. In *Audio Engineering Society Convention 50*. Audio Engineering Society.
- [Gerzon, 1975b] Gerzon, M. A. (1975b). Recording concert hall acoustics for posterity. *Journal of the Audio Engineering Society*, 23(7):569–571.

- [Gerzon, 1985] Gerzon, M. A. (1985). Ambisonics in multichannel broadcasting and video. *Journal of the Audio Engineering Society*, 33(11):859–871.
- [Grondin et al., 2019] Grondin, F., Glass, F., Sobieraj, I., and Plumbley, M. D. (2019). Sound event localization and detection using crnn on pairs of microphones. In *Proceedings of the Detection and Classification of Acoustic Scenes and Events 2019 Workshop (DCASE2019)*, pages 84–88, New York University, NY, USA.
- [Haas, 1972] Haas, H. (1972). The influence of a single echo on the audibility of speech. *Journal of the Audio Engineering Society*, 20(2):146–159.
- [Habets and Gannot, 2007] Habets, E. A. P. and Gannot, S. (2007). Generating sensor signals in isotropic noise fields. *The Journal of the Acoustical Society of America*, 122(6):3464–3470.
- [Habets and Gannot, 2010] Habets, E. A. P. and Gannot, S. (2010). Comments on generating sensor signals in isotropic noise fields.
- [Helmholz et al., 2019] Helmholz, H., Andersson, C., and Ahrens, J. (2019). Realtime implementation of binaural rendering of high-order spherical microphone array signals. *Fortschritte der Akustik-DAGA 2019*.
- [Ito et al., 2010] Ito, N., Ono, N., Vincent, E., and Sagayama, S. (2010). Designing the Wiener post-filter for diffuse noise suppression using imaginary parts of inter-channel cross-spectra. In *2010 IEEE International Conference on Acoustics, Speech and Signal Processing*, pages 2818–2821, Dallas, TX, USA. IEEE.
- [Jarrett et al., 2017] Jarrett, D. P., Habets, E. A., and Naylor, P. A. (2017). *Theory and applications of spherical microphone array processing*, volume 9. Springer.

- [Jukić et al., 2015] Jukić, A., van Waterschoot, T., Gerkmann, T., and Doclo, S. (2015). Group sparsity for mimo speech dereverberation. In *2015 IEEE Workshop on Applications of Signal Processing to Audio and Acoustics (WASPAA)*, pages 1–5. IEEE.
- [Kapka and Lewandowski, 2019] Kapka, S. and Lewandowski, M. (2019). Sound source detection, localization and classification using consecutive ensemble of crnn models. *arXiv preprint arXiv:1908.00766*.
- [Kuttruff, 2016] Kuttruff, H. (2016). *Room acoustics*. Crc Press.
- [Liutkus et al., 2017] Liutkus, A., Stöter, F.-R., Rafii, Z., Kitamura, D., Rivet, B., Ito, N., Ono, N., and Fontecave, J. (2017). The 2016 signal separation evaluation campaign. In Tichavský, P., Babaie-Zadeh, M., Michel, O. J., and Thirion-Moreau, N., editors, *Latent Variable Analysis and Signal Separation - 12th International Conference, LVA/ICA 2015, Liberec, Czech Republic, August 25-28, 2015, Proceedings*, pages 323–332, Cham. Springer International Publishing.
- [Löllmann et al., 2019] Löllmann, H. W., Brendel, A., and Kellermann, W. (2019). Comparative study for single-channel algorithms for blind reverberation time estimation. In *Proc. Intl. Congress on Acoustics (ICA)*.
- [Looney and Gaubitch, 2020] Looney, D. and Gaubitch, N. D. (2020). Joint estimation of acoustic parameters from single-microphone speech observations. In *ICASSP 2020-2020 IEEE International Conference on Acoustics, Speech and Signal Processing (ICASSP)*, pages 431–435. IEEE.
- [Madmoni and Rafaely, 2018] Madmoni, L. and Rafaely, B. (2018). Direction of arrival estimation for reverberant speech based on enhanced decomposition of the direct sound. *IEEE Journal of Selected Topics in Signal Processing*, 13(1):131–142.

- [Majdak et al., 2013] Majdak, P., Iwaya, Y., Carpentier, T., Nicol, R., Parmentier, M., Roginska, A., Suzuki, Y., Watanabe, K., Wierstorf, H., Ziegelwanger, H., et al. (2013). Spatially oriented format for acoustics: A data exchange format representing head-related transfer functions. In *Audio Engineering Society Convention 134*. Audio Engineering Society.
- [Majdak and Noisternig, 2015] Majdak, P. and Noisternig, M. (2015). Aes69-2015: Aes standard for file exchange-spatial acoustic data file format. *Audio Engineering Society*.
- [Malham, 2003] Malham, D. (2003). Higher order ambisonic systems. *Abstracted from "Space in Music-Music in Space", an Mphil thesis by Dave Malham, submitted to the University of York in April*.
- [McCowan and Bourlard, 2003] McCowan, I. and Bourlard, H. (2003). Microphone array post-filter based on noise field coherence. *IEEE Transactions on Speech and Audio Processing*, 11(6):709–716.
- [Merimaa and Pulkki, 2005] Merimaa, J. and Pulkki, V. (2005). Spatial impulse response rendering i: Analysis and synthesis. *Journal of the Audio Engineering Society*, 53(12):1115–1127.
- [Mesaros et al., 2019] Mesaros, A., Adavanne, S., Politis, A., Heittola, T., and Virtanen, T. (2019). Joint measurement of localization and detection of sound events. In *IEEE Workshop on Applications of Signal Processing to Audio and Acoustics (WASPAA)*, New Paltz, NY, USA.
- [Mesaros et al., 2018] Mesaros, A., Heittola, T., and Virtanen, T. (2018). A multi-device dataset for urban acoustic scene classification. In *Proceedings of the Detection and Classification of Acoustic Scenes and Events 2018 Workshop (DCASE2018)*, pages 9–13.
- [Moreau et al., 2006] Moreau, S., Daniel, J., and Bertet, S. (2006). 3d sound field recording with higher order ambisonics—objective

measurements and validation of a 4th order spherical microphone. In *120th Convention of the AES*, pages 20–23.

- [Motlicek et al., 2013] Motlicek, P., Duffner, S., Korchagin, D., Bourlard, H., Scheffler, C., Odobez, J.-M., Del Galdo, G., Kallinger, M., and Thiergart, O. (2013). Real-Time Audio-Visual Analysis for Multiperson Videoconferencing. *Advances in Multimedia*, 2013:1–21.
- [Murphy et al., 2017] Murphy, D., Shelley, S., Foteinou, A., Brereton, J., and Daffern, H. (2017). Acoustic heritage and audio creativity: the creative application of sound in the representation, understanding and experience of past environments.
- [Nguyen et al., 2020] Nguyen, T. N. T., Jones, D. L., and Gan, W.-S. (2020). A sequence matching network for polyphonic sound event localization and detection. In *Proc. IEEE ICASSP*, pages 71–75. IEEE.
- [Noisternig et al., 2003] Noisternig, M., Sontacchi, A., Musil, T., and Holdrich, R. (2003). A 3d ambisonic based binaural sound reproduction system. In *Audio Engineering Society Conference: 24th International Conference: Multichannel Audio, The New Reality*. Audio Engineering Society.
- [OpenAIRlib, 2020] OpenAIRlib (2020). The open acoustic impulse response library. www.openairlib.net. Accessed on June 26th, 2020.
- [P. Habets et al., 2006] P. Habets, E., Gannot, S., and Cohen, I. (2006). Dual-Microphone Speech Dereverberation in a Noisy Environment. In *2006 IEEE International Symposium on Signal Processing and Information Technology*, pages 651–655, Vancouver, BC, Canada. IEEE.

- [Panayotov et al., 2015] Panayotov, V., Chen, G., Povey, D., and Khudanpur, S. (2015). Librispeech: an asr corpus based on public domain audio books. In *2015 IEEE International Conference on Acoustics, Speech and Signal Processing (ICASSP)*, pages 5206–5210. IEEE.
- [Pedregosa et al., 2011] Pedregosa, F., Varoquaux, G., Gramfort, A., Michel, V., Thirion, B., Grisel, O., Blondel, M., Prettenhofer, P., Weiss, R., Dubourg, V., Vanderplas, J., Passos, A., Cournapeau, D., Brucher, M., Perrot, M., and Duchesnay, E. (2011). Scikit-learn: Machine learning in Python. *Journal of Machine Learning Research*, 12:2825–2830.
- [Pérez-López and de Muynke, 2018] Pérez-López, A. and de Muynke, J. (2018). Ambisonicsdrir. <https://github.com/andresperezlopez/AmbisonicsDRIR>. Accessed on June 26th, 2020.
- [Pérez-López et al., 2019] Pérez-López, A., Fonseca, E., and Serra, X. (2019). A hybrid parametric-deep learning approach for sound event localization and detection. In *Proceedings of the Detection and Classification of Acoustic Scenes and Events 2019 Workshop (DCASE2019)*, pages 189–193, New York University, NY, USA.
- [Pérez-López and Politis, 2020] Pérez-López, A. and Politis, A. (2020). A python library for multichannel acoustic signal processing. In *Proc. 148th Audio Engineering Society Convention*. Audio Engineering Society.
- [Politis, 2016] Politis, A. (2016). *Microphone array processing for parametric spatial audio techniques*. PhD thesis, Aalto University.
- [Politis, 2020] Politis, A. (2020). Github repository. <https://github.com/polarch>. Accessed on June 26th, 2020.

- [Politis et al., 2020] Politis, A., Adavanne, S., and Virtanen, T. (2020). A dataset of reverberant spatial sound scenes with moving sources for sound event localization and detection. *arXiv e-prints: 2006.01919*.
- [Politis et al., 2015] Politis, A., Delikaris-Manias, S., and Pulkki, V. (2015). Direction-of-arrival and diffuseness estimation above spatial aliasing for symmetrical directional microphone arrays. In *2015 IEEE International Conference on Acoustics, Speech and Signal Processing (ICASSP)*, pages 6–10, South Brisbane, Queensland, Australia. IEEE.
- [Politis et al., 2018] Politis, A., Tervo, S., and Pulkki, V. (2018). COMPASS: Coding and Multidirectional Parameterization of Ambisonic Sound Scenes. In *2018 IEEE International Conference on Acoustics, Speech and Signal Processing (ICASSP)*, pages 6802–6806, Calgary, AB. IEEE.
- [Postma et al., 2016] Postma, B. N., Poirier-Quinot, D., Meyer, J., and Katz, B. F. (2016). Virtual reality performance auralization in a calibrated model of notre-dame cathedral. *Euroregio*, 6:1–10.
- [Prego et al., 2012] Prego, T. d. M., de Lima, A. A., Netto, S. L., Lee, B., Said, A., Schafer, R. W., and Kalker, T. (2012). A blind algorithm for reverberation-time estimation using subband decomposition of speech signals. *The Journal of the Acoustical Society of America*, 131(4):2811–2816.
- [Pulkki, 2006] Pulkki, V. (2006). Directional audio coding in spatial sound reproduction and stereo upmixing. In *Audio Engineering Society Conference: 28th International Conference: The Future of Audio Technology—Surround and Beyond*. Audio Engineering Society.
- [Pulkki, 2007] Pulkki, V. (2007). Spatial sound reproduction with directional audio coding. *Journal of the Audio Engineering Society*, 55(6):503–516.

- [Pulkki et al., 2018] Pulkki, V., Delikaris-Manias, S., and Politis, A. (2018). *Parametric time-frequency domain spatial audio*. Wiley Online Library.
- [PYPL, 2020] PYPL (2020). Pypl popularity of programming language. Accessed on June 26th, 2020.
- [Rafaely, 2004] Rafaely, B. (2004). Analysis and design of spherical microphone arrays. *IEEE Transactions on speech and audio processing*, 13(1):135–143.
- [Rafaely, 2015] Rafaely, B. (2015). *Fundamentals of spherical array processing*, volume 8. Springer.
- [Robinson, 2017] Robinson, D. (2017). The overflow: The incredible growth of python. <https://stackoverflow.blog/2017/09/06/incredible-growth-python/>. Accessed on June 26th, 2020.
- [Romblom, 2017] Romblom, D. (2017). Diffuse field modeling using physically-inspired decorrelation filters: Improvements to the filter design method. *Journal of the Audio Engineering Society*, 65(11):943–953.
- [Rudrich and Frank, 2019] Rudrich, D. and Frank, M. (2019). Improving externalization in ambisonic binaural decoding. In *DAGA 2019 Fortschritte der Akustik*.
- [Sabine, 1927] Sabine, W. C. (1927). *Collected papers on acoustics*. Harvard University Press Cambridge, MA.
- [Särkkä et al., 2004] Särkkä, S., Vehtari, A., and Lampinen, J. (2004). Rao-blackwellized monte carlo data association for multiple target tracking. In *Proceedings of the Seventh International Conference on Information Fusion*, volume 1, pages 583–590, Stockholm, Sweden.

- [Scheibler et al., 2018] Scheibler, R., Bezzam, E., and Dokmanić, I. (2018). Pyroomacoustics: A python package for audio room simulation and array processing algorithms. In *2018 IEEE International Conference on Acoustics, Speech and Signal Processing (ICASSP)*, pages 351–355. IEEE.
- [Schörkhuber and Höldrich, 2017] Schörkhuber, C. and Höldrich, R. (2017). Ambisonic microphone encoding with covariance constraint. In *Proceedings of the International Conference on Spatial Audio*, pages 7–10.
- [Schroeder, 1965] Schroeder, M. R. (1965). New method of measuring reverberation time. *The Journal of the Acoustical Society of America*, 37(6):1187–1188.
- [SOFA, 2018] SOFA (Accessed on March 12th, 2018). Sofa conventions. https://www.sofaconventions.org/mediawiki/index.php/SOFA_conventions.
- [Stanzial et al., 1996] Stanzial, D., Prodi, N., and Schiffrer, G. (1996). Reactive acoustic intensity for general fields and energy polarization. *The Journal of the Acoustical Society of America*, 99(4):1868–1876.
- [Stefanakis and Mouchtaris, 2015] Stefanakis, N. and Mouchtaris, A. (2015). Foreground suppression for capturing and reproduction of crowded acoustic environments. In *2015 IEEE International Conference on Acoustics, Speech and Signal Processing (ICASSP)*, pages 51–55, South Brisbane, Queensland, Australia. IEEE.
- [TheVerge, 2018] TheVerge (2018). Former vr film company jaunt is giving up on vr to focus on augmented reality. <https://www.theverge.com/2018/10/15/17980420/jaunt-vr-layoffs-ar-focus-switch-restructuring-xr-platform>. Accessed on June 11th, 2020.

- [Thiergart et al., 2011] Thiergart, O., Galdo, G. D., and Habets, E. A. P. (2011). Diffuseness estimation with high temporal resolution via spatial coherence between virtual first-order microphones. In *2011 IEEE Workshop on Applications of Signal Processing to Audio and Acoustics (WASPAA)*, pages 217–220, New Paltz, NY, USA. IEEE.
- [Thiergart et al., 2009] Thiergart, O., Schultz-Amling, R., Del Galdo, G., Mahne, D., and Kuech, F. (2009). Localization of sound sources in reverberant environments based on directional audio coding parameters. In *Audio Engineering Society Convention 127*. Audio Engineering Society.
- [Tho et al., 2014] Tho, N. T. N., Zhao, S., and Jones, D. L. (2014). Robust doa estimation of multiple speech sources. In *Proc. IEEE ICASSP*, pages 2287–2291, Florence, Italy. IEEE.
- [Time, 2015] Time (2015). The surprising joy of virtual reality. <https://time.com/3987059/in-the-latest-issue-41/>. Accessed on June 11th, 2020.
- [TIOBE, 2020] TIOBE (2020). Tiobe index for june 2020. <http://www.tiobe.com>. Accessed on June 26th, 2020.
- [Trowitzsch et al., 2019] Trowitzsch, I., Taghia, J., Kashef, Y., and Obermayer, K. (2019). The nigen general sound events database. *arXiv preprint arXiv:1902.08314*.
- [Wikipedia, 2020] Wikipedia (2020). List of ambisonic hardware. https://en.wikipedia.org/wiki/List_of_Ambisonic_hardware. Accessed on June 11th, 2020.
- [Zotter and Frank, 2019] Zotter, F. and Frank, M. (2019). *Ambisonics*. Springer.